Computers and Geotechnics 127 (2020) 103760

Contents lists available at ScienceDirect

Computers and Geotechnics

journal homepage: www.elsevier.com/locate/compgeo

Research Paper

A unified critical state constitutive model for cyclic behavior of silty sands

Xiao Wei[1], Yuan Chen, Jun Yang*

Department of Civil Engineering, The University of Hong Kong, Hong Kong

ARTICLE INFO

Keywords:
Constitutive modeling
Silty sand
Liquefaction
Critical state
State parameter

ABSTRACT

The cyclic behavior of silty sands is complex in that it depends not only on packing density and confining pressure but also on fines content. How to properly model the behavior is emerging as an active area of research in geomechanics and engineering. This paper presents an attempt to formulate a critical state-based constitutive model for describing the cyclic loading behavior of sand with varying fines content. Based on several important experimental findings from recent studies, a unified characterization of the state-dependent elastic modulus and plastic hardening modulus is proposed such that only one set of elastic and hardening parameters is required for sand with varying fines content. By comparing with systematic experimental data, it is shown that the model can produce reasonably good predictions for undrained cyclic responses of silty sands under a range of void ratios, effective confining stresses and fines contents. In particular, the model successfully predicts the experimentally observed variations of sand behavior with fines content under cyclic loading.

1. Introduction

It is widely accepted that the cyclic behavior of sands is dependent on the initial state which is commonly described by packing density and confining pressure. The fines content (FC) is another important factor that can change the mechanical behavior and liquefaction resistance of sands. The effect of fines can be either beneficial or detrimental as shown by several previous laboratory investigations (Shen et al., 1977; Kuerbis et al., 1988; Thevanayagam et al., 2000; Carraro et al., 2003; Xenaki and Athanasopoulos, 2003; Dash and Sitharam, 2009; Stamatopoulos, 2010); the contradictory effects are partly due to the use of different density variables for comparison (Yang et al., 2015). Based on a detailed analysis of different density variables, Yang et al. (Yang et al., 2015) suggested that the usual global void ratio (e) remains a proper and simple density variable as compared with the skeleton void ratio and the equivalent inter-granular void ratio. When compared at the same post-consolidation global void ratio, the presence of non-plastic fines is to increase the liquefaction potential (Yang et al., 2015; Yang and Wei, 2012) and decrease the cyclic resistance ratio (*CRR*) (Wei and Yang, 2019) of clean sand, as shown in Fig. 1 for Toyoura sand mixed with crushed silica silt. More recently, several laboratory studies have also found that the elastic shear modulus (*G*) of sand tends to decrease with the addition of non-plastic fines (Wichtmann et al., 2015; Yang and Liu, 2016). The effects of fines along with the effects of density and confining stress make it difficult to characterize the behavior of silty sand with varying fines content.

Constitutive modeling of soil behavior under static and cyclic loading has experienced rapid development in the past several decades (Wang et al., 1990; Pastor et al., 1990; Darve and Labanieh, 1982; Borja and Andrade, 2006;195:5115–40.; Li and Dafalias, 2000; Zhang and Wang, 2012; Zhao and Gao, 2016; Wang and Xie, 2014; Wei and Yang, 2019; Jefferies, 1993; Manzari and Dafalias, 1997; Li, 2002; Ling and Liu, 2003; Dafalias and Manzari, 2004; Taiebat and Dafalias, 2008; Dafalias and Taiebat, 2016; Yang et al., 2019; Ling and Yang, 2006). How to simulate the state-dependent behavior of sand has been a critical issue. One of the options is to adopt a state variable in the critical state soil mechanics (CSSM) framework. The state parameter (Been and Jefferies, 1985) appears to be the most widely used state variable for characterizing the mechanical behavior of sands. Several key features of sand behavior, such as onset of flow liquefaction (Yang, 2002) and cyclic liquefaction resistance (Wei and Yang, 2019; Yang and Sze, 2011), can be captured in a reasonable way by using the state parameter. Among the critical state based models, there is a family of models now known as SANISAND (Manzari and Dafalias, 1997; Li and Dafalias, 2012; Dafalias and Manzari, 2004; Taiebat and Dafalias, 2008; Dafalias and Taiebat, 2016), which is featured by the state-dependent bounding surface and flow rule. Although the capability of these models in simulating the mechanical behavior of sand has been well acknowledged, the calibration and validation are mainly based on experimental data on clean sand. When the models are applied to silty

* Corresponding author.
E-mail addresses: weixiaos@connect.hku.hk (X. Wei), u3525376@connect.hku.hk (Y. Chen), junyang@hku.hk (J. Yang).
[1] Currently National University of Singapore, Singapore.

https://doi.org/10.1016/j.compgeo.2020.103760
Received 1 February 2020; Received in revised form 16 July 2020; Accepted 16 July 2020
Available online 31 July 2020
0266-352X/

Nomenclature

List Of Notations

a	Model parameter in K_p
A_e	Fitting parameter of G using F(e)
a_e	Fitting parameter of G in F(e)
A_ψ	Fitting parameter of G using F(ψ)
a_ψ	Fitting parameter of G in F(ψ)
CSL	Critical state line
D	Dilatancy
d_0	Dilatancy parameter
$d\varepsilon_q$	Deviatoric strain increment
$d\varepsilon_q^e$	Elastic deviatoric strain increment
$d\varepsilon_q^p$	Plastic deviatoric strain increment
$d\varepsilon_v$	Volumetric strain increment
$d\varepsilon_v^e$	Elastic volumetric strain increment
$d\varepsilon_v^p$	Plastic volumetric strain increment
e	Void ratio
e_{max}, e_{min}	Maximum and minimum void ratio, respectively
e_0 (e_c)	Void ratio prior to shearing (after consolidation)
e_Γ	Intercept of critical state line in the e-$(p'/P_a)^\xi$ plane
F(e)	Void ratio function
$f(X_1, X_2, X_3\ldots)$	Function of X_1, X_2, $X_3\ldots$
F(ψ)	State parameter function
FC	Fines content (%)
fc	Fines content in decimal
G	Elastic shear modulus
h, h_1, h_2	Hardening parameters
K	Elastic bulk modulus
k	Pressure exponential of modulus
K_p	Plastic hardening modulus
L	Loading index
m	Dilatancy parameter
M	Stress ratio (η) at critical state
n	Hardening parameter
p' (p_c')	Mean effective stress (after consolidation)
P_a	Reference stress equaling to 1 atm
PSD	Particle size distribution
q	Deviatoric stress
R	Roundness
R_{comb}	Combined roundness
α	Parameter of G considering effects of cyclic loading
ε_q	Deviatoric strain
ε_q^e	Elastic deviatoric strain
ε_q^p	Plastic deviatoric strain
ε_v	Volumetric strain
ε_v^e	Elastic volumetric strain
ε_v^p	Plastic volumetric strain
ζ	Accumulated plastic deviatoric strain
η	Stress ratio q/p'
η_{peak}	Peak stress ratio (η)
η_{PTS}	Stress ratio (η) at phase transformation state
λ_c	Magnitude of the slope of CSL
ν	Poisson's ratio of soil
ξ	Pressure exponential of CSL formulation
φ_{cs}	Critical state friction angle
ψ	State parameter
ψ_0 (ψ_c)	Initial state parameter prior to shearing (after consolidation)

sand, FC-specific parameters are generally required, implying that a clean sand mixed with different amounts of fines need to be treated as different materials. This brings significant difficulty since the quantity of fines may vary appreciably even within a single deposit of sand.

In any elasto-plastic model, the elastic modulus is an essential element and it affects the stress-strain relationship through the general stiffness matrix (Potts and Zdravković, 2001; Wood, 1990). A proper description of the elastic behavior of soils plays an important role in performance-based designs of geotechnical structures. A noteworthy finding from a recent laboratory study (Yang and Liu, 2016) is that the elastic shear modulus (G) can be formulated in a more rational way through a state parameter function, F(ψ), instead of the traditional void ratio function F(e). This paper presents an attempt to formulate a simple constitutive model for sand with different percentages of fines by incorporating the state-parameter dependence of elastic modulus along with a state-parameter-dependent plastic hardening modulus. With additional consideration of the cyclic loading induced stiffness change, the cyclic behavior of silty sands can be satisfactorily modeled by the proposed model. In the following sections the formulation, calibration and validation of the model are described in detail.

2. Constitutive framework

For clarity, the model is formulated in the standard triaxial space on the platform of Li and Dafalias (2000), Yang and Li (2004) with the concept of zero elastic zone (Dafalias and Taiebat, 2016). The yield surface $f(p', q, \eta)$ is given as:

$$f(p', q, \eta) = q - p'\eta = 0 \tag{1}$$

where p' is the mean effective stress, q is the deviatoric stress and η ($=q/p'$) is the stress ratio. The concept of zero elastic zone is derived from the wedge-like elastic zone used by earlier versions of SANISAND (Manzari and Dafalias, 1997; Dafalias and Manzari, 2004), as shown in Fig. 2(a). By reducing the size of the elastic zone to infinitely small, the two boundaries of the elastic zone converge to a single line (Fig. 2 (b)) which is expressed by Eq. (1). The loading index (L) is defined as:

$$L = \pm\frac{1}{K_p}\left(\frac{\partial f}{\partial q}\mathrm{d}q + \frac{\partial f}{\partial p'}\mathrm{d}p'\right) = \pm\frac{1}{K_p}p'\mathrm{d}\eta \tag{2}$$

where K_p is the plastic hardening modulus to be defined later; the " ± " sign is used here to account for the processes of increasing and decreasing stress ratio, respectively. A " + " sign is assigned to the process of $\mathrm{d}\eta > 0$ and a " − " is assigned to the process of $\mathrm{d}\eta < 0$. The present model adopts a simplified version of the mapping rule in the q-p' space for conventional triaxial tests. The non-associated flow rule is applied to define the plastic strain increments as follows:

$$\begin{cases} \mathrm{d}\varepsilon_q^p = \frac{1}{K_p}p'\mathrm{d}\eta \\ \mathrm{d}\varepsilon_v^p = D\cdot\mathrm{d}\varepsilon_q^p \end{cases} \tag{3}$$

where $d\varepsilon_q^p$ and $d\varepsilon_v^p$ are the plastic deviatoric strain increment and the plastic volumetric strain increment, respectively; and D is the state dependent dilatancy to be defined later. By assuming additive decomposition of the strain increments, the following equations can be obtained:

$$\begin{Bmatrix} \mathrm{d}\varepsilon_q \\ \mathrm{d}\varepsilon_v \end{Bmatrix} = \begin{bmatrix} \frac{1}{3G} + \frac{1}{K_p} & -\frac{\eta}{K_p} \\ \frac{D}{K_p} & \frac{1}{K} - \frac{D\eta}{K_p} \end{bmatrix} \begin{Bmatrix} \mathrm{d}q \\ \mathrm{d}p' \end{Bmatrix} \tag{4}$$

where $d\varepsilon_q$ and $d\varepsilon_v$ are deviatoric and volumetric strain increments, respectively. Reversing Eq. (4) gives a general elastoplastic constitutive relationship as follows:

$$\begin{Bmatrix} \mathrm{d}q \\ \mathrm{d}p' \end{Bmatrix} = \left(\begin{bmatrix} 3G & 0 \\ 0 & K \end{bmatrix} - \frac{h(L)}{K_p + 3G - K\eta D} \begin{bmatrix} 9G^2 & -3KG\eta \\ 3KGD & -K^2\eta D \end{bmatrix} \right) \begin{Bmatrix} \mathrm{d}\varepsilon_q \\ \mathrm{d}\varepsilon_v \end{Bmatrix} \tag{5}$$

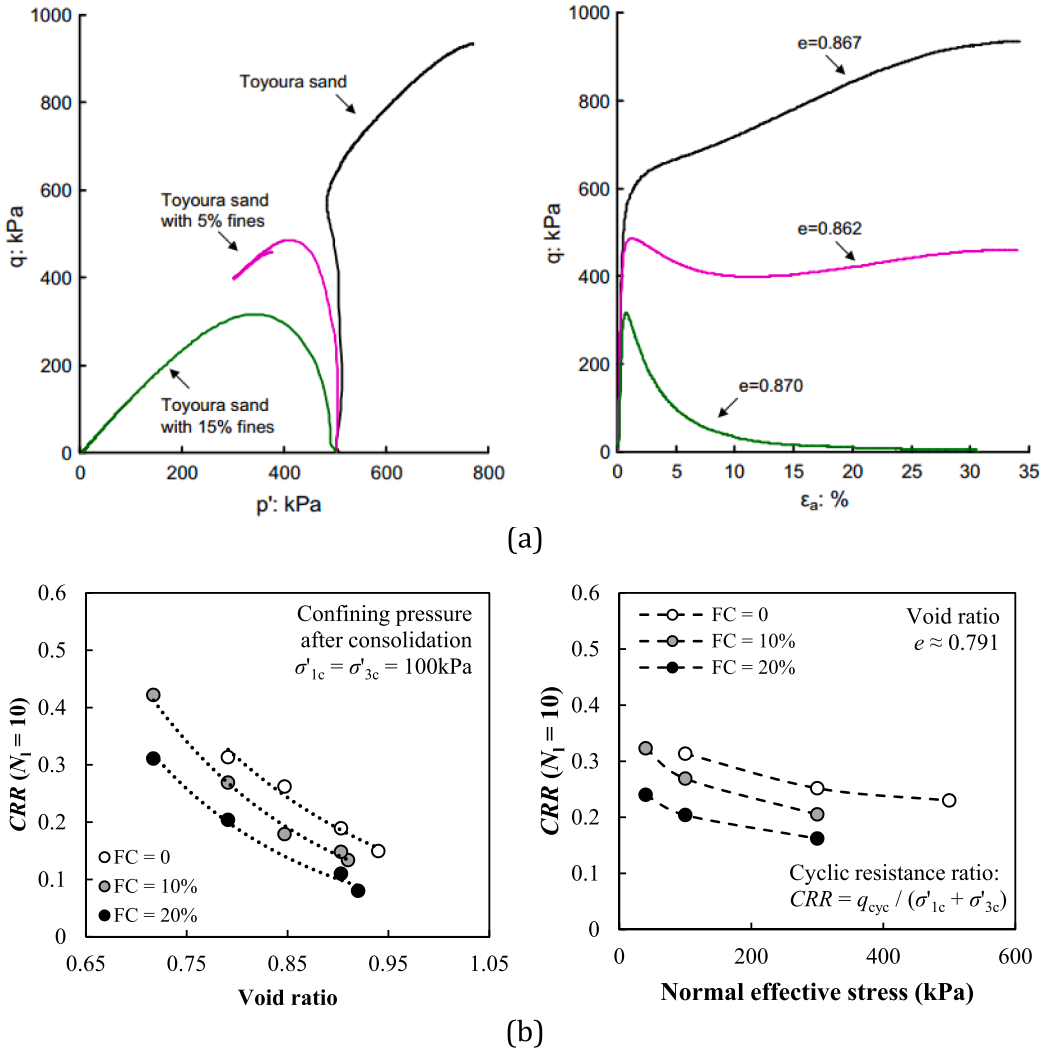

Fig. 1. Effects of fines on the liquefaction potential of sand subjected to (a) monotonic loading (Yang et al., 2015), and (b) cyclic loading (Wei and Yang, 2019).

In addition to the yield surface, the model has three additional surfaces, namely, bounding surface, critical state surface, and dilatancy surface. The stress ratios of these three surfaces are M^b, M, and M^d, respectively (Fig. 2(c)). These three surfaces will be used to define K_p and D.

2.1. Implementation of CSSM

2.1.1. Elastic moduli

The elastic shear modulus of sand (Iwasaki and Tatsuoka, 1977; Wichtmann and Triantafyllidis, 2009) has been widely characterized using the following equation:

$$G = A_e F(e)\left(\frac{p'}{p_a}\right)^k = A_e \frac{(a_e - e)^2}{1+e}\left(\frac{p'}{p_a}\right)^k \tag{6}$$

where A_e, a_e and k are fitting parameters, p_a is the atmospheric pressure. Laboratory studies have found that the elastic stiffness varies with the addition of non-plastic fines (Wichtmann et al., 2015; Yang and Liu, 2016). For instance, the elastic shear modulus (G) decreases with increasing fines content (up to a threshold fines content of ~30%) when compared at the same post-consolidation void ratio and confining stress, as shown in Fig. 3(a) for Toyoura sand mixed with different percentages of silica silt. This implies that a constitutive model using the traditional void ratio formulation of elastic modulus (e.g., Eq. (6)) requires FC-specific model parameters, as shown in Fig. 3(b) that the parameter A_e is a function of FC.

When measured G values are plotted as a function of the state parameter (ψ), corresponding to the post-consolidation state, the effect of fines content can be unified such that G decreases with increasing ψ (Fig. 4). This important finding eventually leads to a state-parameter dependent elastic shear modulus as follows (Yang and Liu, 2016):

$$G = A_\psi F(\psi)\left(\frac{p'}{P_a}\right)^k = A_\psi \frac{(a_\psi - \psi)^2}{1+\psi}\left(\frac{p'}{P_a}\right)^k \tag{7a}$$

where A_ψ, a_ψ, and k are fitting parameters. Yang and Liu (2016) have shown that the notion of ψ-dependent shear modulus applies to different sand-fines mixtures including a natural silty sand (Huang et al., 2004). Wei and Yang (2019) have successfully implemented Eq. (7a) into a model to simulate the monotonic behavior of silty sands.

To account for the effects of cyclic loading on the small-strain shear modulus as revealed by the laboratory investigation (Goto et al., 1999), an additional term, $(p'/p_c')^\alpha$, is introduced to the expression of G, as follows,

$$G = A_\psi \frac{(a_\psi - \psi)^2}{1+\psi}\left(\frac{p'}{P_a}\right)^k \left(\frac{p'}{p_c'}\right)^\alpha \tag{7b}$$

where p_c' is the mean effective stress after consolidation and α is an empirical model parameter. For compliance with monotonic simulation, it is suggested to apply Eq. (7a) to the loading process before the

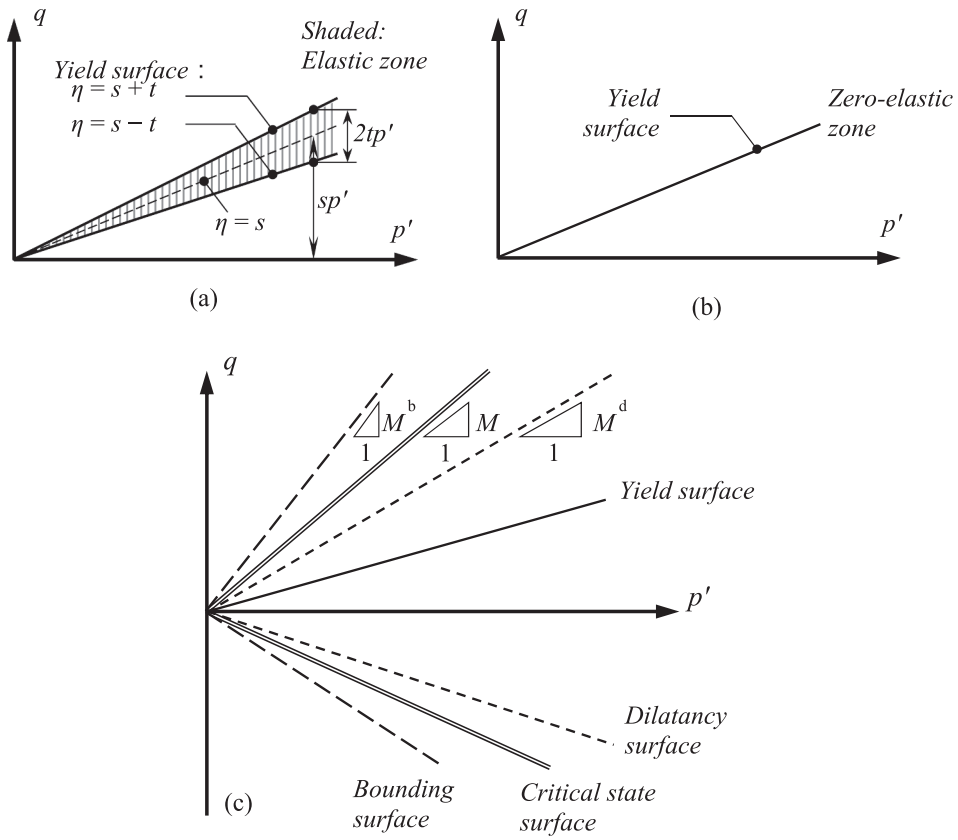

Fig. 2. (a) Wedge-like elastic zone adopted by Manzari and Dafalias (1997); (b) zero-elastic zone adopted by Dafalias and Taiebat (2016) and the present study; (c) model surfaces in the q-p' space.

first reversal of $d\eta$. In the case of uniform stress cycles, Eq. (7a) is applicable to the first quarter of the first cycle, while Eq. (7b) is applied to stress cycles after the first reversal of $d\eta$. The added term, $(p'/p_c')^{\alpha}$, is useful in capturing the large strain development during cyclic mobility when the effective stress approaches zero upon the reversal of cyclic shear stress.

The elastic bulk modulus, K, can be obtained by measuring the compressional wave velocity, and the dependence of K on the state parameter is anticipated. Alternatively, K can be obtained by the following equation:

$$K = G\frac{2(1+\nu)}{3(1-2\nu)} \tag{8}$$

where ν is Poisson's ratio. With a commonly-assumed constant ν, a state-parameter dependent K is straightforward.

2.1.2. Dilatancy

The dilatancy, D, is state parameter dependent as follows:

$$D = \frac{d_0}{M}[\pm M^d - \eta] \tag{9a}$$

$$M^d = M\exp(m\psi) \tag{9b}$$

where d_0 and m are model parameters; the ' $\pm$ ' sign indicates that it depends on the loading process, which is '+' for $d\eta > 0$ and '−' for $d\eta < 0$. During the process of $d\eta > 0$, D is initially positive when η is small. Because this process is associated with a positive $d\varepsilon_q^p$, a positive $d\varepsilon_v^p$ is obtained representing a contractive plastic volumetric increment. As η increases, negative D is obtained yielding a dilatant plastic volumetric increment. During the process of $d\eta < 0$, a negative D is obtained initially associated with a negative $d\varepsilon_q^p$, thus yielding a contractive plastic volumetric increment ($d\varepsilon_v^p > 0$). As η decreases and becomes negative, positive D can be obtained in association with a negative $d\varepsilon_q^p$, yielding a dilatant plastic volumetric increment ($d\varepsilon_v^p < 0$).

2.1.3. Plastic hardening modulus

The plastic hardening modulus, K_p, is given as follows to capture the softening response of sands:

$$K_p = \frac{hG\exp(n\psi)}{\eta - \eta_{in}}[\pm M^b - \eta] \tag{10a}$$

$$M^b = M\exp(-n\psi) \tag{10b}$$

where η_{in} is the stress ratio at the latest state where $d\eta$ reverses its sign, either from "+" to "−", or from "−" to "+"; h and n are model parameters; the ' $\pm$ ' sign takes '+' for $d\eta > 0$ and '−' for $d\eta < 0$. During the process of $d\eta > 0$, K_p is initially positive when η is small. Once η is large enough yielding $M^b - \eta < 0$, strain-softening takes place with a negative K_p. During the process of $d\eta < 0$, K_p is initially positive when η is small, since $-M^b - \eta < 0$ and $\eta - \eta_{in} < 0$. As η keeps decreasing and becomes negative, strain-softening may take place when $-M^b - \eta > 0$.

The parameter h is the hardening parameter which was originally proposed as a function of the initial void ratio (Li and Dafalias, 2000) as follows:

$$h = h_1 - h_2 e_0 \tag{11}$$

where h_1 and h_2 are two positive fitting parameters and e_0 is the initial void ratio. To model the monotonic behavior of silty sands, Wei and Yang (2019) proposed the following linear equation to characterize the unique relationship between h and the initial state parameter (ψ_0), regardless of different fines contents,

$$h = h_1 - h_2\psi_0 \tag{12}$$

where the values of h_1 and h_2 are different from those in Eq. (11). In this

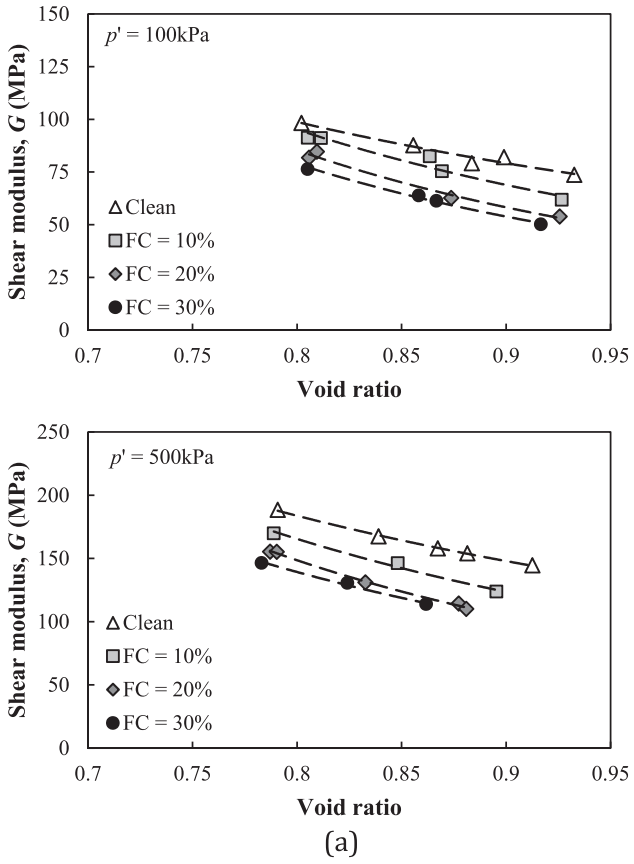

Fig. 3. (a) FC-specific *G-e* relationships (Yang and Liu, 2016); (b) variation of parameter A_e with increasing fines content (Yang and Liu, 2016).

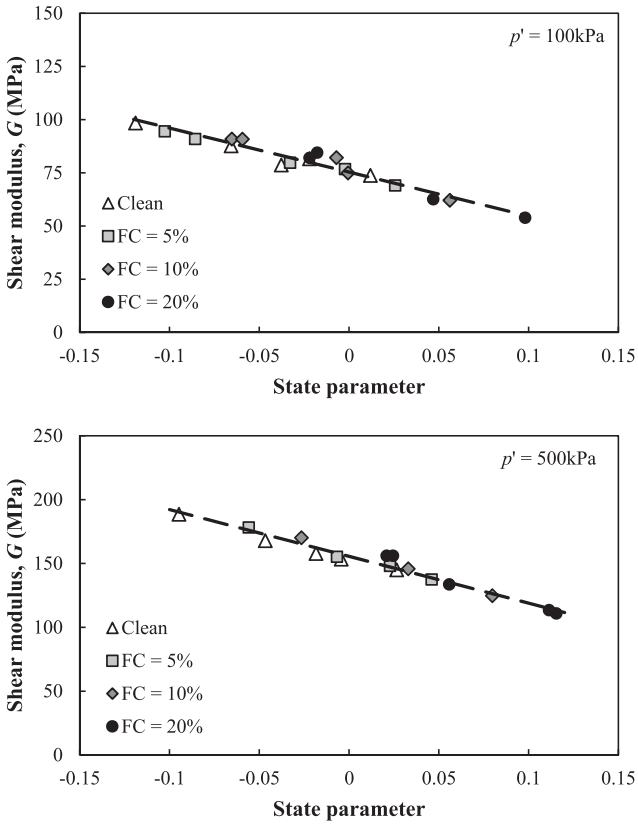

Fig. 4. FC-unified elastic *G-ψ* relationship for different confining pressures (Yang and Liu, 2016).

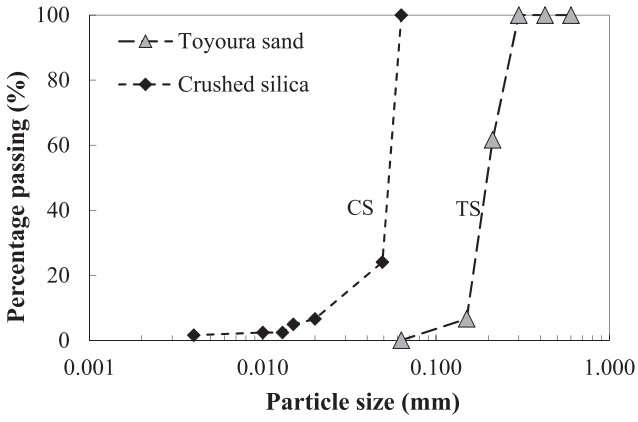

Fig. 5. Particle size distribution curves of Toyoura sand and crushed silica silt.

regard, both the elastic modulus and the plastic hardening modulus are state-parameter dependent and unified for different fines contents. In addition, to incorporate the effects of accumulated plastic strain on the plastic hardening modulus and to facilitate the simulation of the undrained cyclic response of sands (Wei and Yang, 2019), K_p may be further modified as follows:

$$K_p = \frac{1}{1+a\zeta}\frac{hG\exp(n\psi)}{\eta-\eta_{in}}[\pm M^b - \eta] \tag{13}$$

where a is a positive fitting parameter, ζ is the accumulated plastic deviatoric strain to be calculated using the following equation.

$$\zeta = \int |d\varepsilon_q^p| \tag{14}$$

Table 1
Monotonic tests for model calibration (Liang, 2016).

Test ID	*FC* (%)	e_c	p_c': kPa	ψ_0
TS-IC015	0	0.928	500	0.044
TS-IC016	0	0.894	500	0.010
TS-IC017	0	0.878	500	−0.006
TSS10-IC007	10	0.880	300	0.037
TSS10-IC009	10	0.880	500	0.062
TSS10-IC010	10	0.901	500	0.083
TSS20-IC007	20	0.846	500	0.082
TSS20-IC010	20	0.834	300	0.043

Table 2
Calibrated parameters for moist-tamped Toyoura sand mixed with crushed silica silt.

Critical state				Elastic		Dilatancy		Hardening	
FC	0	10%	20%						
e_Γ	0.9427	0.9117	0.8657	A_ψ (kPa)	15,000	d_o	0.88	h_1	6.6
λ_c	0.0225	0.0357	0.0388	a_ψ	1.36	m	3.5	h_2	30.56
ξ	0.6	0.6	0.6	k	0.4			n	1.1
M	1.21	1.24	1.29	ν	0.2			a	500
				α	0.58				

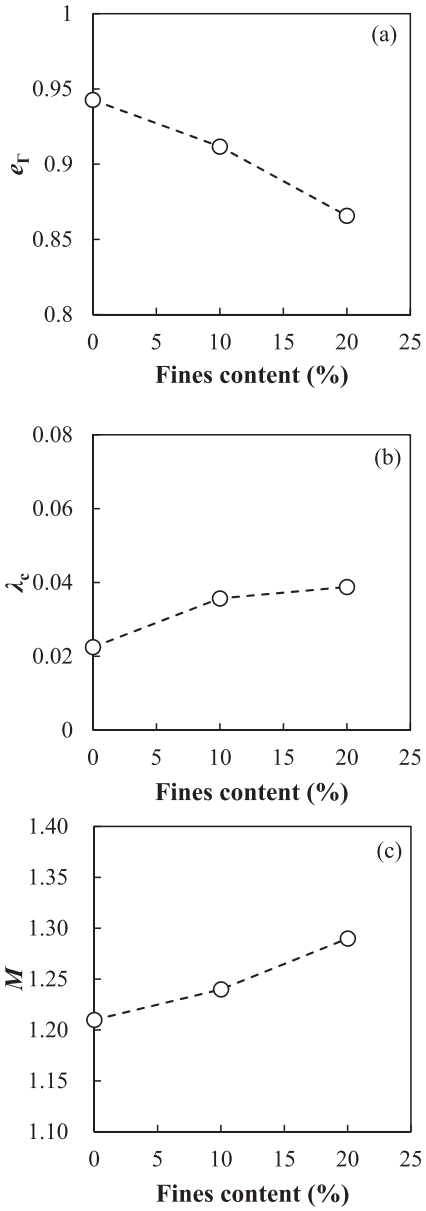

Fig. 6. Calibrated critical state parameters of Toyoura sand mixed with crushed silica silt.

3. Model calibration

The model calibration is demonstrated using a series of monotonic triaxial tests on mixtures of Toyoura sand and crushed silica silt (Yang and Liu, 2016; Liang, 2016). The particle size distribution curves of the sand and the fines are presented in Fig. 5. In the laboratory tests, the specimens were prepared by the moist-tamping method. Table 1 summarizes the laboratory tests for model calibration and Table 2 summarizes the calibrated model parameters.

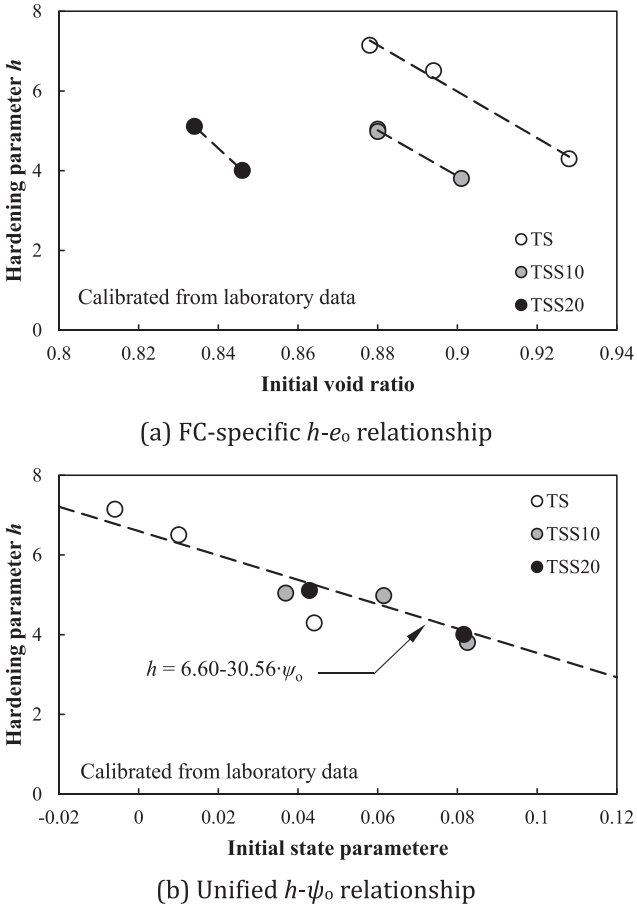

Fig. 7. Hardening parameter h as a function of (a) initial void ratio, and (b) initial state parameter.

Table 3
Calibrated parameters for moist-tamped Sydney sand mixed with low plastic fines.

Critical state			Elastic		Dilatancy		Hardening	
FC	15%	30%						
e_Γ	0.666	0.546	A_ψ (kPa)	10,000	d_o	0.5	h_1	1
λ_c	0.029	0.048	a_ψ	2.17	m	1	h_2	1.13
ξ	0.6	0.6	k	0.75			n	1.1
M	1.305	1.305	ν	0.15			a	30
			α	0.13				

3.1. Critical state parameters

The critical state parameters are determined from laboratory testing. The critical state line in the e-p' plane is represented by a power law as follows (Li and Wang, 1998; Yang and Li, 2004):

$$e = e_\Gamma - \lambda_c \left(\frac{p'}{P_a}\right)^\xi \tag{15}$$

where e_Γ is the intercept in the e-$(p'/P_a)^\xi$ plane, λ_c is the magnitude of the slope and ξ is the pressure exponent with a typical value ranging from 0.6 to 0.8. The e_Γ and λ_c of silty sands were found to be functions of fines content (Yang and Wei, 2012) as shown in Fig. 6(a) and (b) and

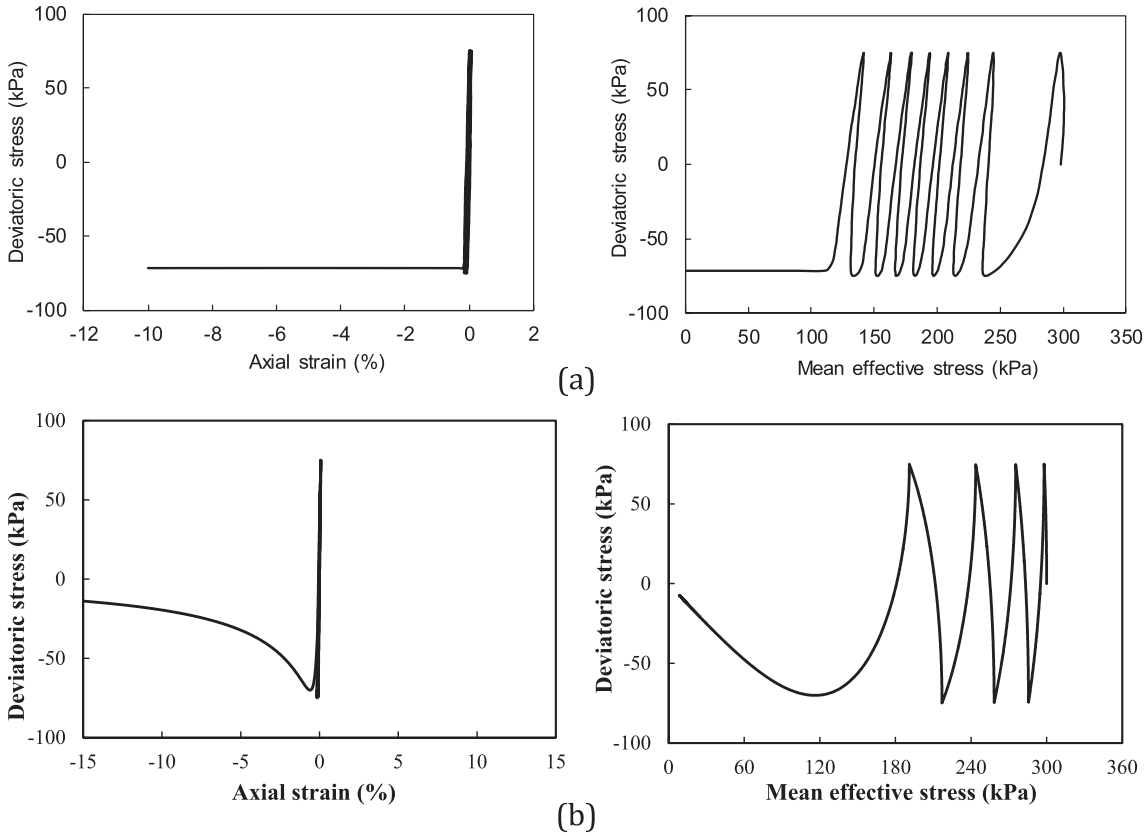

Fig. 8. Flow failure of clean Toyoura sand ($e_c \approx 0.940$, $p_c' = 300$ kPa, $q_{cyc} = 75$ kPa): (a) experimental result (Yang and Sze, 2011); and (b) simulation.

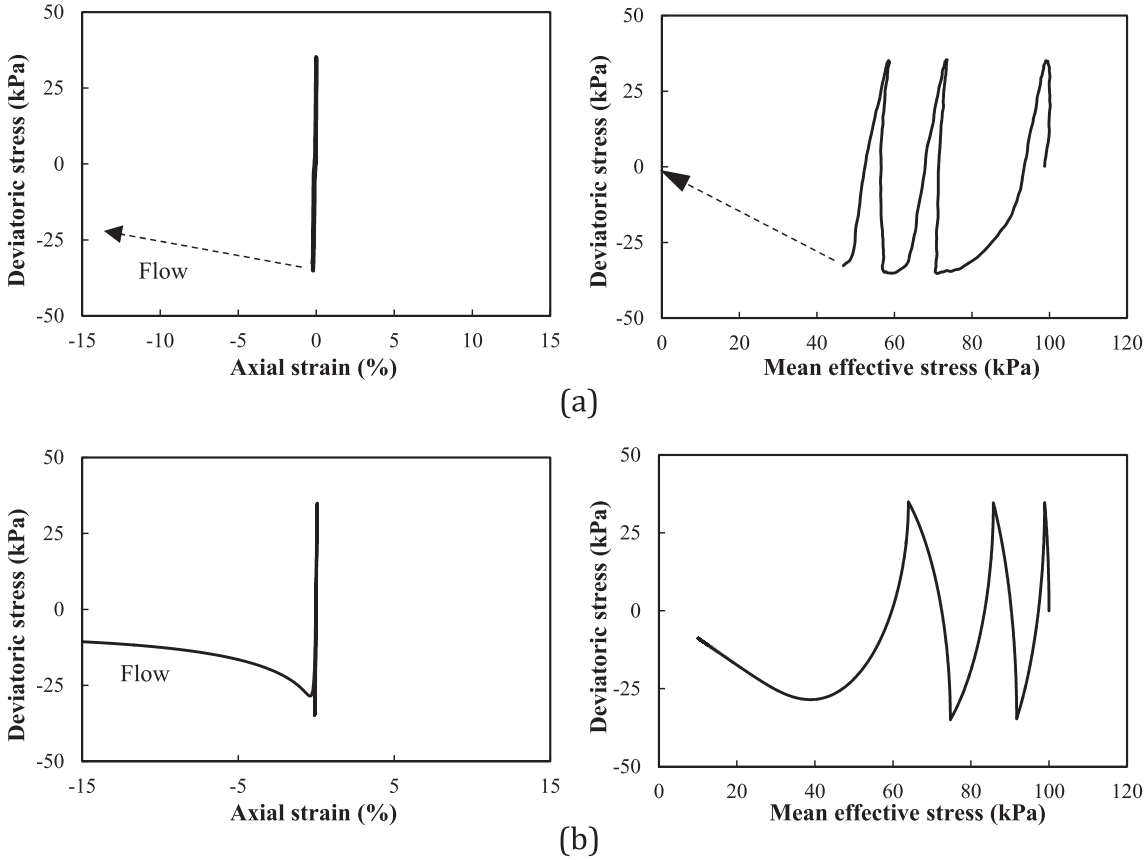

Fig. 9. Flow failure of TSS10 ($e_c \approx 0.903$, $p_c' = 100$ kPa, $q_{cyc} = 35$ kPa): (a) experimental result; and (b) simulation.

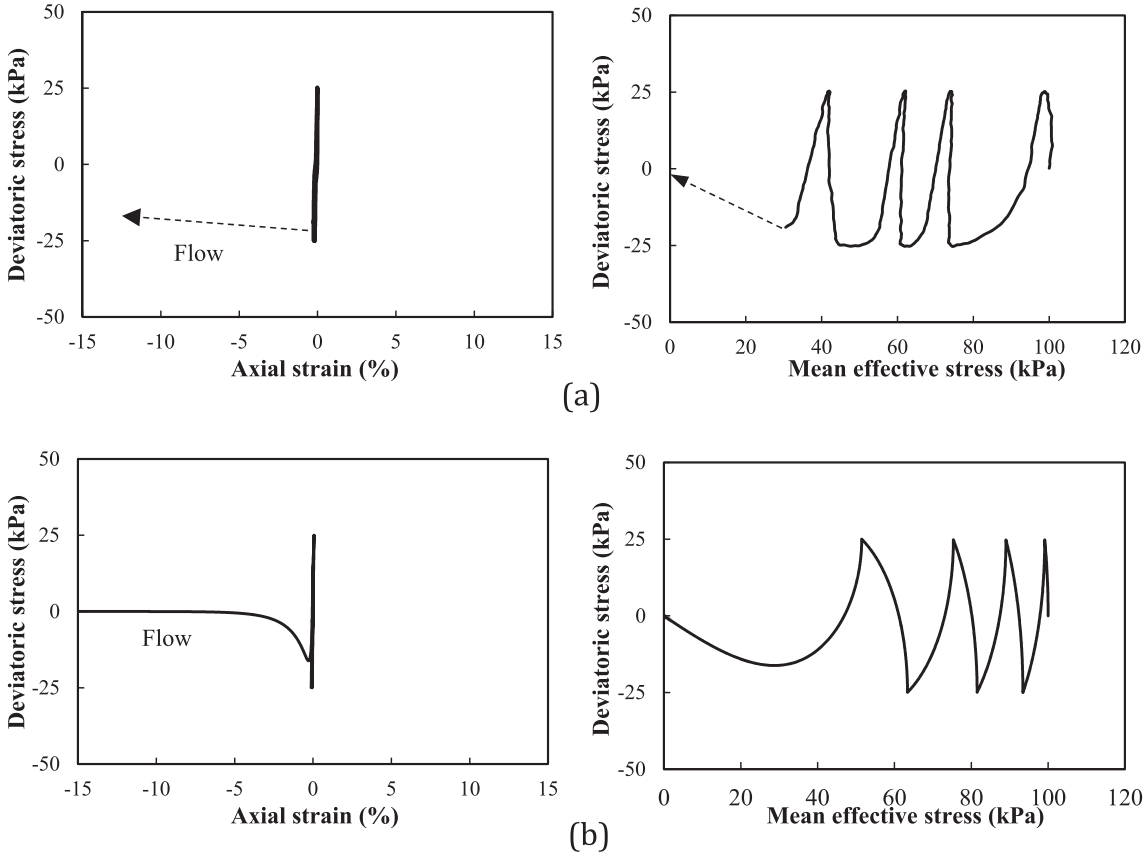

Fig. 10. Flow failure of TSS20 ($e_c \approx 0.903$, $p_c' = 100$ kPa, $q_{cyc} = 25$ kPa): (a) experimental result; and (b) simulation.

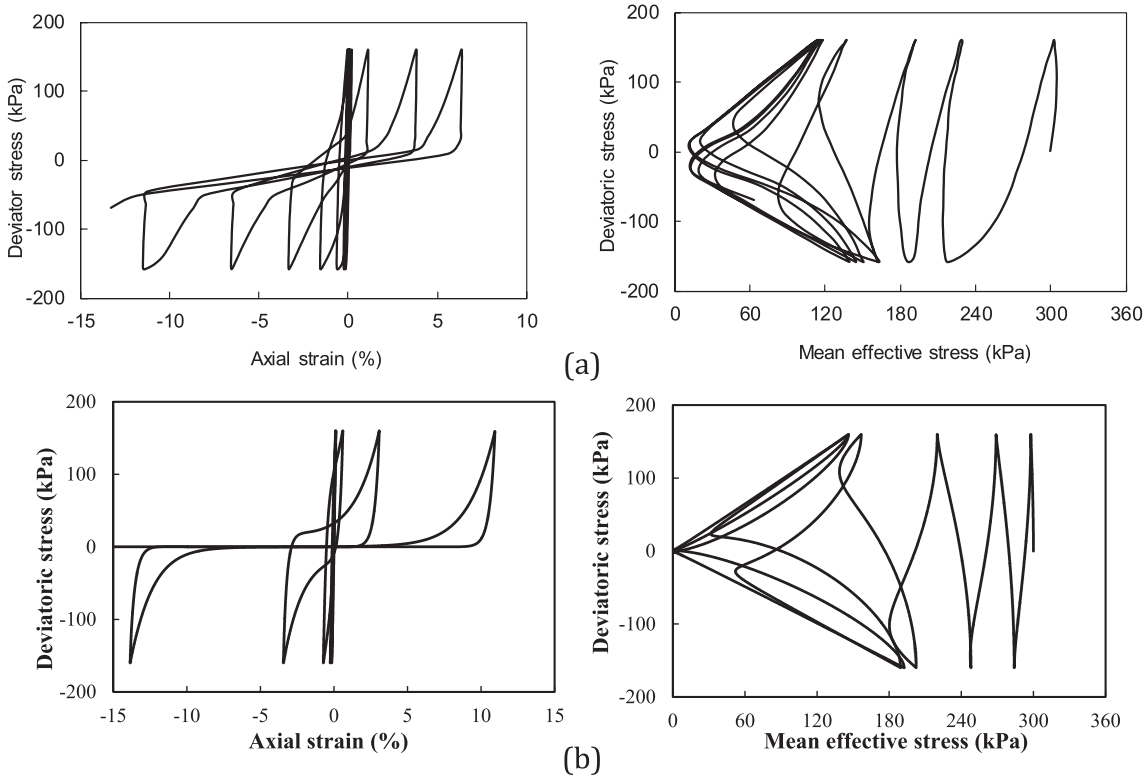

Fig. 11. Cyclic mobility of clean Toyoura sand ($e_c \approx 0.791$, $p_c' = 300$ kPa, $q_{cyc} = 160$ kPa): (a) experimental result (Yang and Sze, 2011); and (b) simulation.

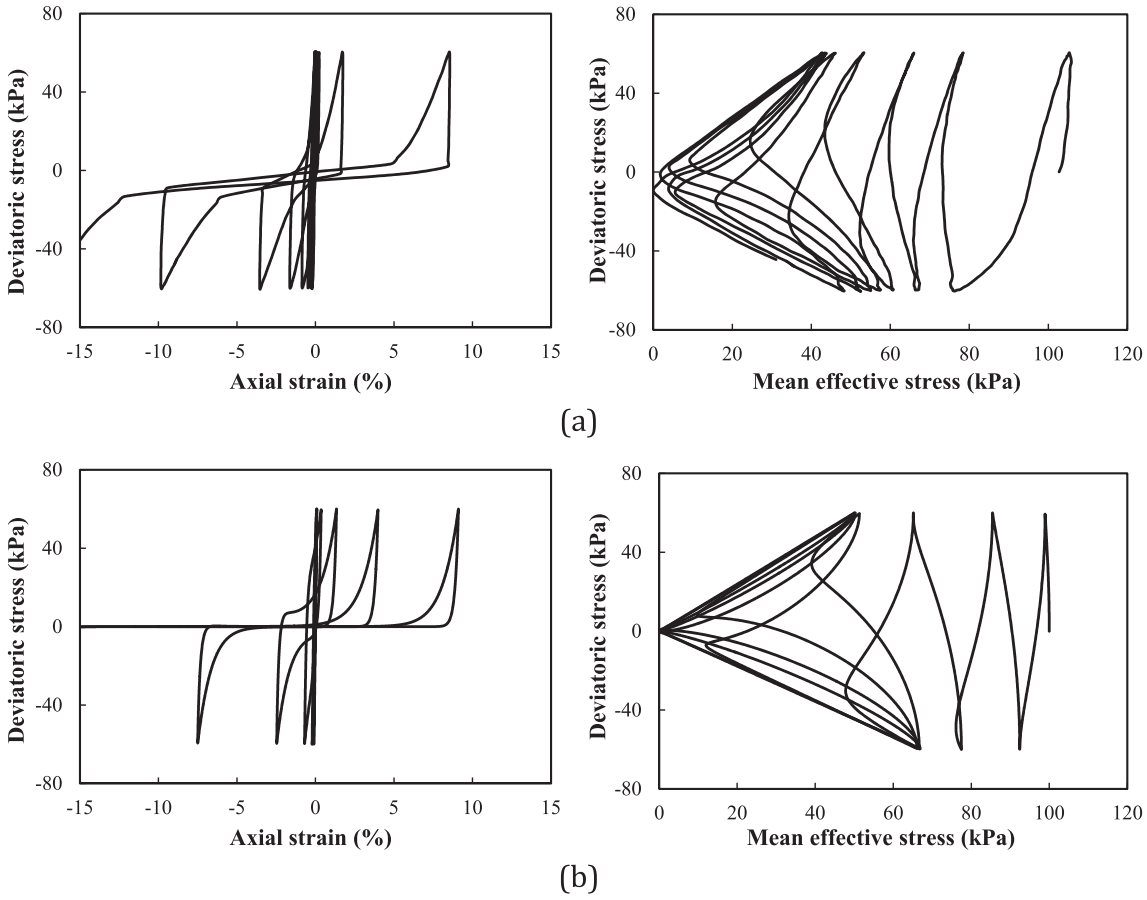

Fig. 12. Cyclic mobility of TSS10 ($e_c \approx 0.791$, $p_c' = 100$ kPa, $q_{cyc} = 60$ kPa): (a) experimental result; and (b) simulation.

thus can be estimated by some empirical methods (Stamatopoulos et al., 2015) after the critical state line of the base sand is determined. The exponent ξ is taken as 0.6 in this study, which is the best-fitted value from the test data of Yang and Wei (2012), Liang (2016).

The critical state stress ratio, M, is determined by triaxial compression tests in this study. It is related to the critical state friction angle (φ_{cs}), which is affected by the roundness (R) of sand particles (Yang and Luo, 2015). The concept of combined roundness, R_{comb} (Yang and Wei, 2012), defined below, is useful for characterizing φ_{cs} of silty sands:

$$R_{comb} = R_{sand}\cdot(1 - fc) + R_{fines}\cdot fc \tag{16}$$

where fc is the fines content in decimal. This implies that M can be a function of FC for a given series of sand-fine mixtures (Fig. 6(c)).

3.2. Elastic properties

Theoretically, the elastic shear modulus should be calibrated using bender element tests or resonant column tests at very small strain level. In many studies, however, the shear modulus of Toyoura sand was calibrated using conventional triaxial test data (Li and Dafalias, 2000). This explains why these studies used much lower shear moduli than those determined using resonant column tests (Yang and Liu, 2016). It should be noted that the elastic shear modulus determined by resonant column test can result in a very stiff stress-strain response, i.e. attainment of characteristic states such as undrained instability state and phase transformation state at relative small strain levels. Manzari and Dafalias (1997), Papadimitriou et al. (2001) also noticed this problem and suggested to reduce the shear modulus from small-strain measurements by a factor of 2 to 3. In this study, a reduced value of $A_\psi = 15{,}000$ kPa is used, instead of 41,330 kPa by resonant column tests (Yang and Liu, 2016). In fact, Wei and Yang (2019) have suggested a reduction factor to account for the effects of stress ratio on shear modulus, through which the shear modulus measured by small-strain techniques can be applied.

Since G has been calibrated, K can be determined using Eq. (8) with Poisson's ratio. Gu et al. (2013) reported that Poisson's ratio of Touyora sand ranges from 0.2 to 0.25 depending on void ratio and mean effective stress. For simplicity, the Poisson's ratio is assumed to be a constant for the series of silty sands with different fines contents.

3.3. Dilatancy parameters

The parameter m can be determined by using monotonic triaxial test data when $D = 0$ at the phase transformation state ($\eta = \eta_{PTS}$). Then m can be solved as follows.

$$m = \frac{1}{\psi_d}\ln\left(\frac{\eta_{PTS}}{M}\right) \tag{17}$$

where ψ_d is the state parameter at phase transformation state. The parameter d_0 can be determined by drained triaxial tests as suggested by Li and Dafalias (2000) or by undrained triaxial tests (Wei and Yang, 2019). Firstly, the incremental plastic strains are calculated by Eq. (18a) and (18b).

$$d\varepsilon_q^p = d\varepsilon_q - \frac{dq}{3G} \tag{18a}$$

$$d\varepsilon_v^p = d\varepsilon_v - \frac{dp'}{G}\frac{3(1-2\nu)}{2(1+\nu)} \tag{18b}$$

Then the value of d_0 can be obtained by fitting the relationship between D and $[M\cdot\exp(m\psi)\text{-}\eta]/M$ as suggested by the following equation.

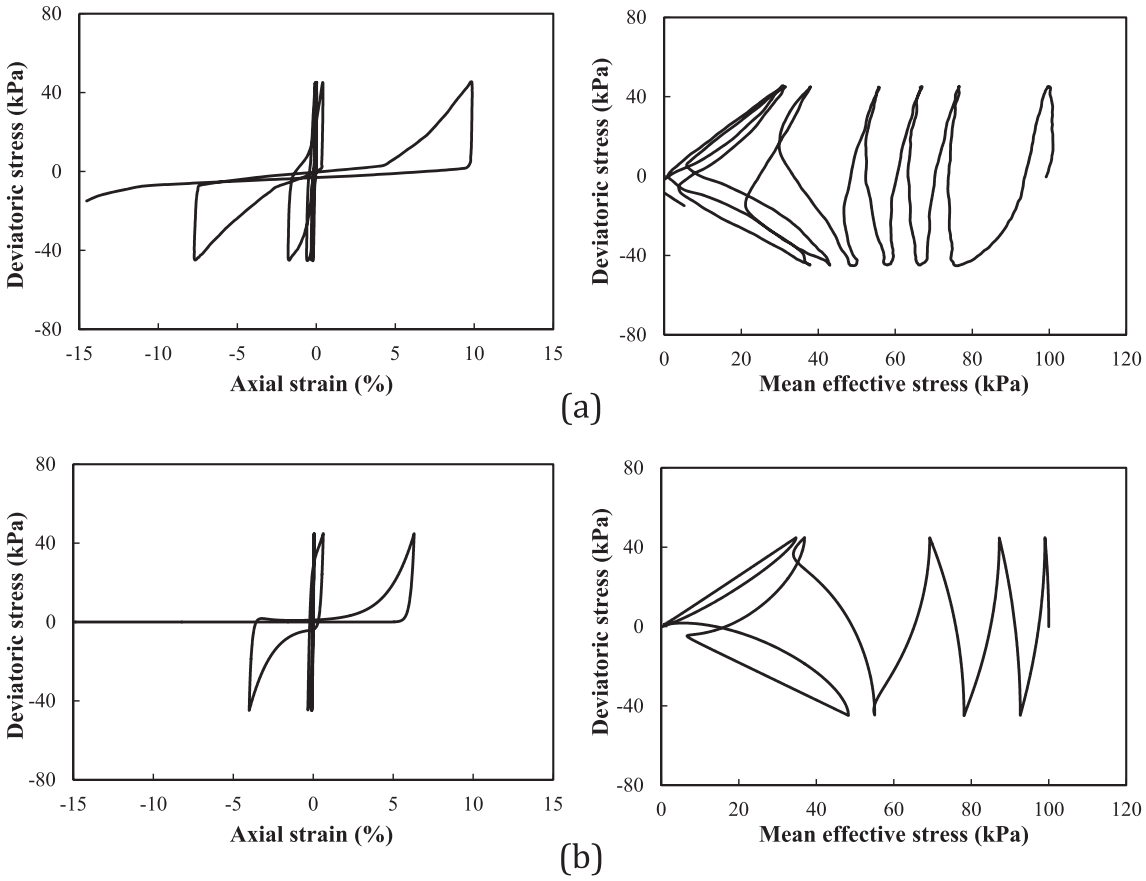

Fig. 13. Cyclic mobility of TSS20 ($e_c \approx 0.791$, $p_c' = 100$ kPa, $q_{cyc} = 45$ kPa): (a) experimental result; and (b) simulation.

$$D = \frac{d\varepsilon_v^p}{d\varepsilon_q^p} = d_0 \frac{M\exp(m\psi) - \eta}{M} \tag{19}$$

The values of m and d_0 may vary for different fines contents (Wei and Yang, 2019), and the dilatancy relationship is dependent on the particle shape and the gradational properties (including FC) of the sand (Guo and Su, 2007; Simoni and Houlsby, 2006; Xiao et al., 2014). Nevertheless, a single set of m and d_0 can be used for different FCs to produce well acceptable results (Table 2).

3.4. Hardening parameters

The parameter n can be determined by the following equation, which is derived from $K_p = 0$ when the peak stress ratio state is attained ($\eta = \eta_{peak}$) during a drained triaxial test:

$$n = \frac{1}{\psi_{peak}} \ln\left(\frac{M}{\eta_{peak}}\right) \tag{20}$$

where ψ_{peak} is the state parameter at the peak state. The hardening parameter n is chosen to be constant for various fines contents because it has relatively minor influence on the simulation results.

The parameter h can be determined by either drained or undrained triaxial tests (Li and Dafalias, 2000). Using undrained triaxial data, h can be solved by the following equation:

$$\frac{dq}{dp'} = \eta - \frac{K_p}{KD} = \eta - \frac{h}{d_o}\frac{M\exp(n\psi)}{\eta}\frac{M\exp(-n\psi) - \eta}{M\exp(m\psi) - \eta}\frac{3(1-2\nu)}{2(1+\nu)}\frac{1}{1+a\zeta} \tag{21}$$

It is more straightforward if Eq. (21) is rearranged as follows:

$$V = h \cdot H \tag{22}$$

where

$$V = \left(\eta - \frac{dq}{dp'}\right)\frac{d_0}{M}[M\exp(m\psi) - \eta]\frac{2(1+\nu)}{3(1-2\nu)} \tag{23}$$

$$H = \frac{1}{1+a\zeta}\frac{\exp(n\psi)}{\eta}[M\exp(-n\psi) - \eta] \tag{24}$$

The parameter h can be obtained by plotting V against H. As shown in Fig. 7(a), h decreases with increasing void ratio and exhibits a FC-specific h-e_0 relationship, thus implying that sand-fine mixtures with different fines contents should be treated as different materials. However, a unique trend between h and ψ_0 (Fig. 7(b)) is found by plotting against the initial state parameter (ψ_0), regardless of fines content and confining pressure. This state-parameter dependent relationship of h requires only a single set of h_1 and h_2. In this regard, both the elastic modulus and the plastic hardening modulus are state-parameter dependent and unified for different fines contents.

4. Validations

The validation of model is performed for two series of sand-fine mixtures, namely the Toyoura sand series (Wei and Yang, 2019; Yang and Sze, 2011) and the Sydney sand series (Rahman et al., 2014; Baki et al., 2012). The test results of Toyoura sand series were generated from mixtures of Toyoura sand and crushed silica silt, with the fines content varying from 0 to 20%. The specimens were prepared by the moist-tamping method and loaded under uniform deviatoric stresses with a sinusoidal waveform after they were saturated and consolidated. The samples of Sydney sand series were also prepared by the moist-tamping method. Sydney sand is clean uniform silica sand, while the fines is a mixture of Majura fines and commercial kaolin with a plastic

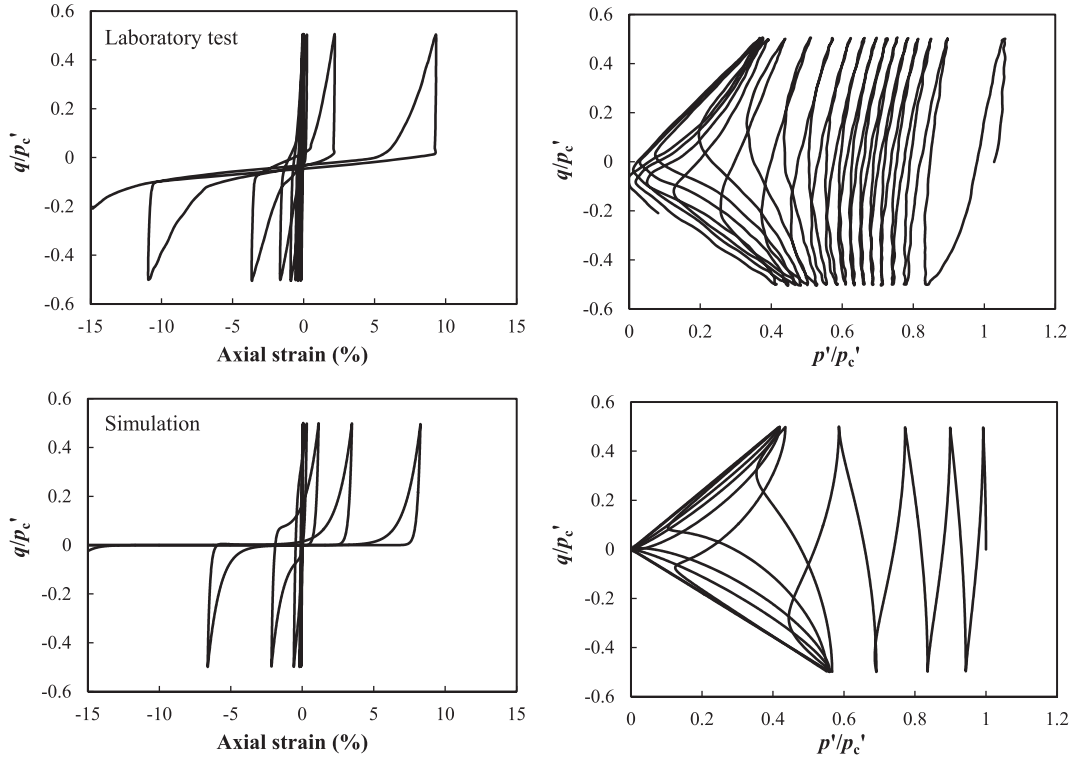

(a) TSS10, $e_c \approx 0.791$, $p_c' = 100$kPa, $q_{cyc}/p_c' = 0.5$

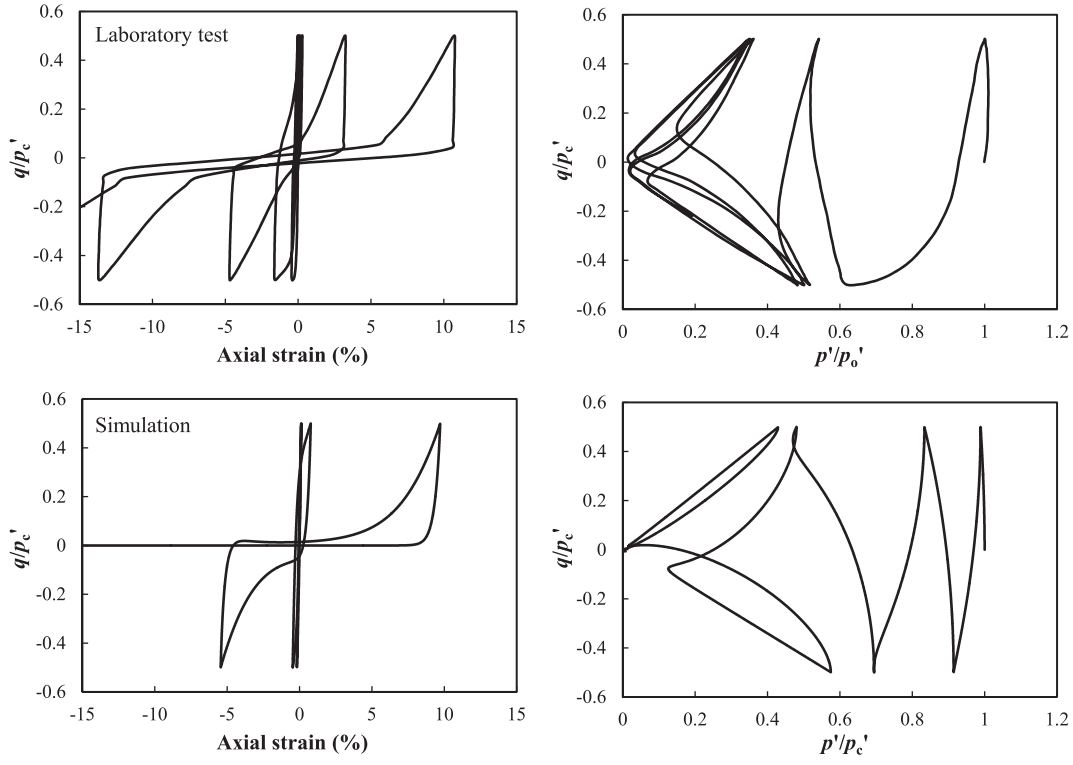

(b) TSS10, $e_c \approx 0.791$, $p_c' = 300$kPa, $q_{cyc}/p_c' = 0.5$

Fig. 14. Effects of effective confining stress on cyclic behavior.

index of 27. The undrained cyclic responses are simulated using the calibrated parameters in Tables 2 and 3 for various initial conditions and fines contents.

4.1. Toyoura sand series

The undrained cyclic behavior can be generally categorized into two types, namely, flow type behavior (flow failure) and non-flow type

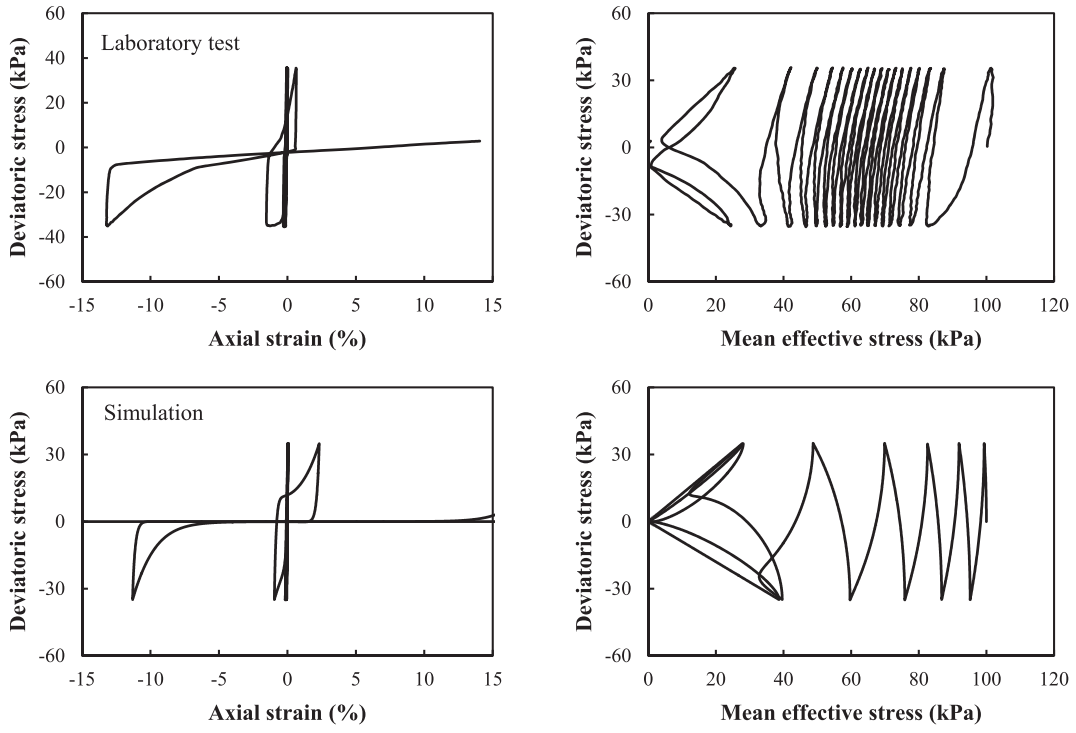

(a) TSS10, e_c = 0.847, p_c' = 100kPa, q_{cyc}/p_c' = 0.35

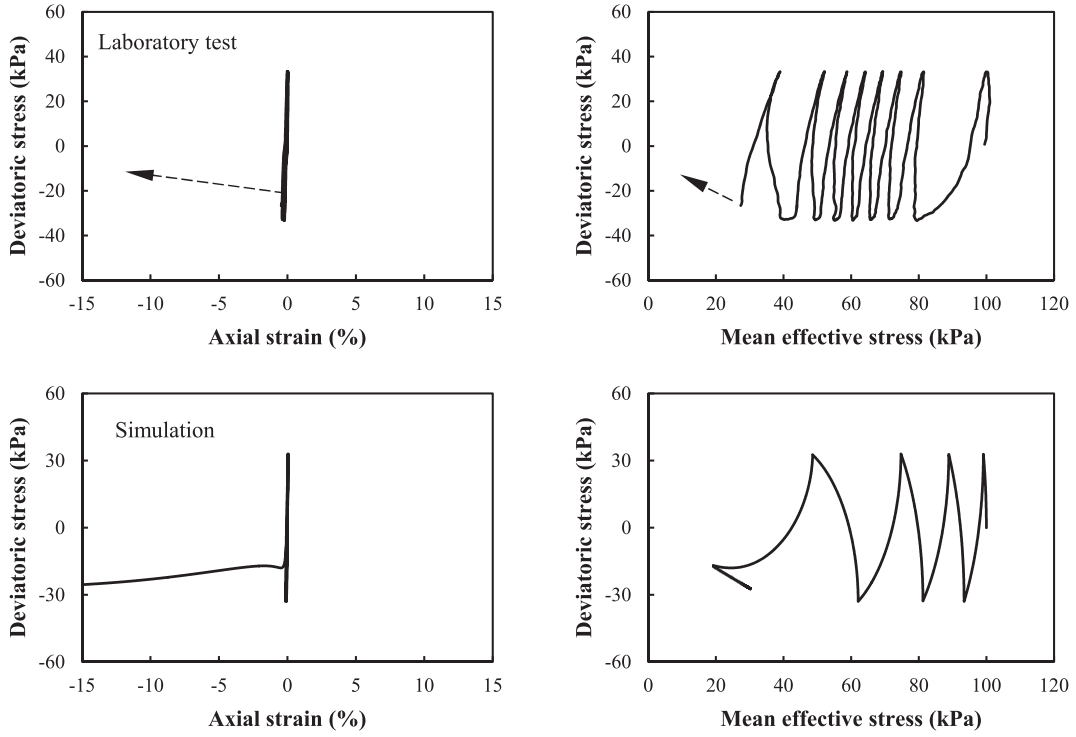

(b) TSS20, e_c = 0.847, p_c' = 100kPa, q_{cyc}/p_c' = 0.33

Fig. 15. Effects of fines content on cyclic behavior.

behavior (cyclic mobility) (Wei and Yang, 2019; Yang and Sze, 2011; Sze and Yang, 2014). The flow type behavior is common in very loose specimens and is characterized by a sudden loss of strength and a rapid development of deformation. Cyclic mobility, the non-flow type behavior, takes place in medium dense to dense specimens. It is characterized by progressively increasing strains associated with the transient liquefied state when the shear stress reverses its direction. More detailed categorization and description of failure patterns can be found in Sze and Yang (2014).

4.1.1. *Prediction of flow type behavior*

Three typical tests exhibiting flow type behavior are simulated using

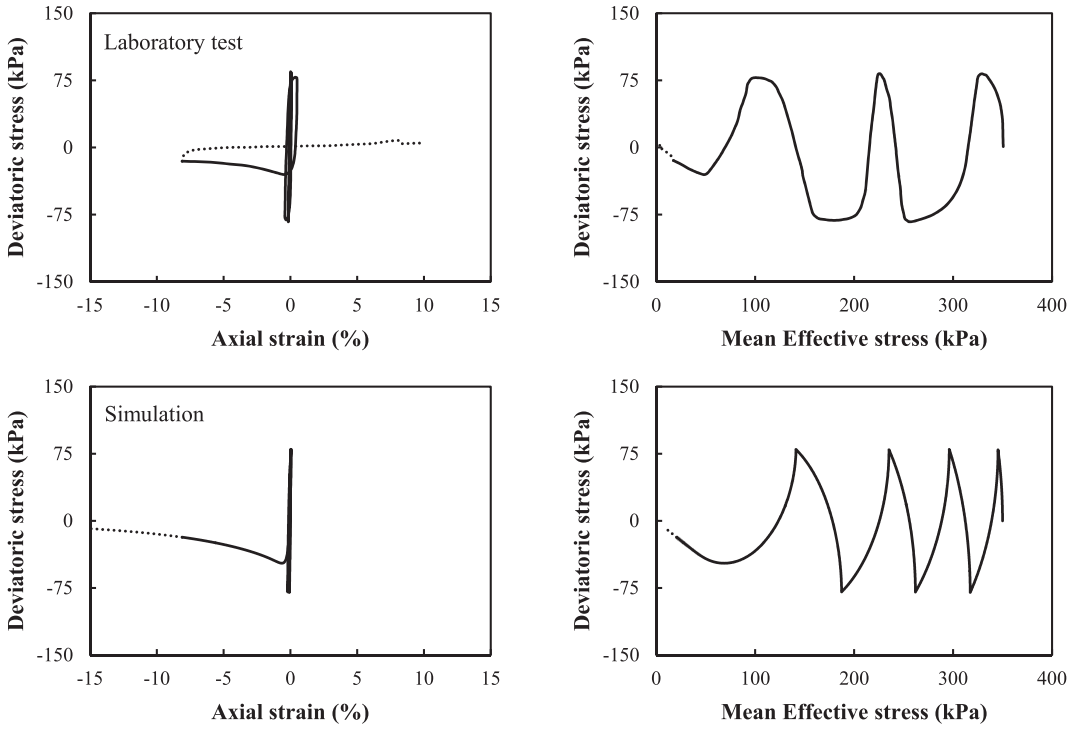

(a) C-15-144, FC = 15%, e_c = 0.676, p_c' = 350 kPa

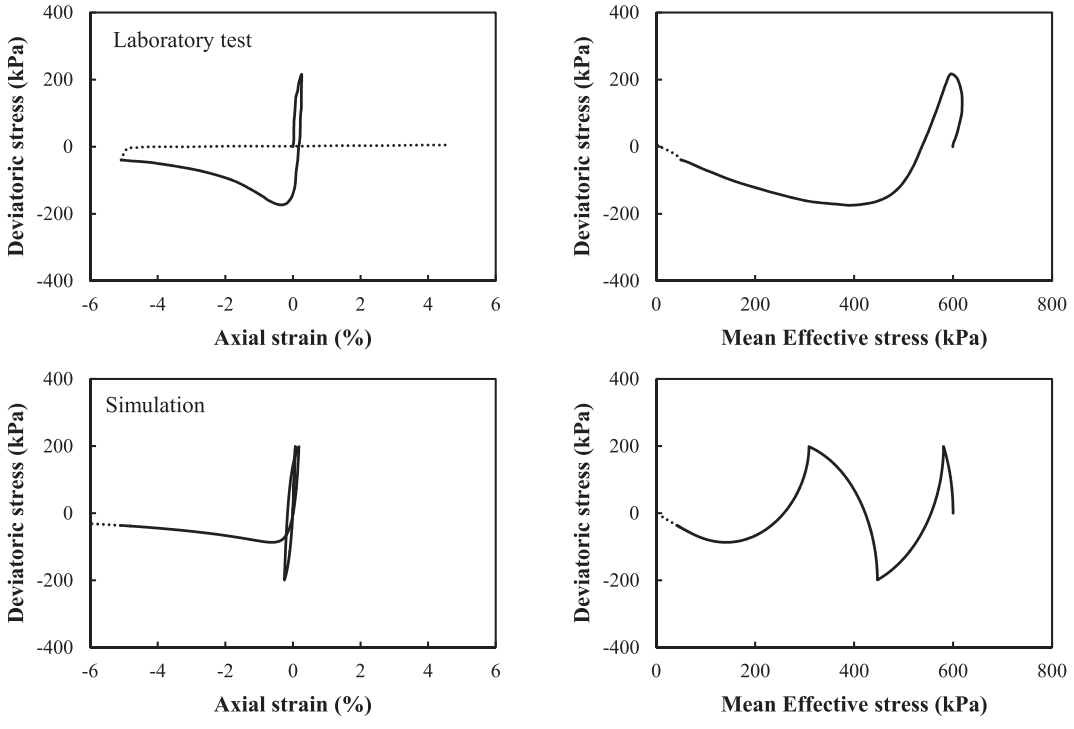

(b) C-15-51, FC = 15%, e_c = 0.670, p_c' = 600 kPa

Fig. 16. Flow failure of Sydney sand series (laboratory data extracted from Rahman et al. (2014), Baki et al. (2012)).

the proposed model, which correspond to three cases of fines contents, i.e., FC = 0 (Fig. 8), 10% (Fig. 9) and 20% (Fig. 10). In the laboratory all the specimens were prepared at a relatively loose state ($e_c \approx$ 0.903–0.940). Overall, the agreement between simulations and experiments is satisfactory. It is worth noting that the laboratory tests were conducted under stress-controlled conditions and as a consequence, the abrupt and rapid development of deformation associated with flow type failure could not be recorded. The simulations are, however, performed under a strain-controlled mode and the stress-strain response and the stress path during flow can be predicted.

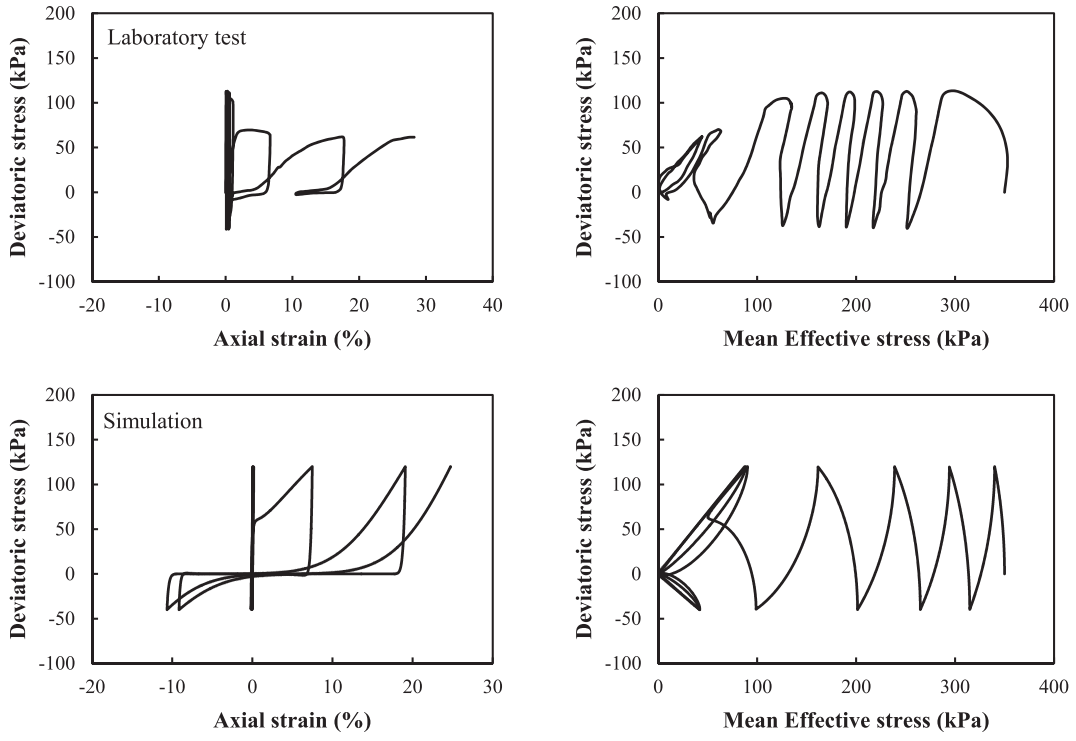

(a) C-30-61, FC = 30%, e_c = 0.487, p_c' = 350 kPa

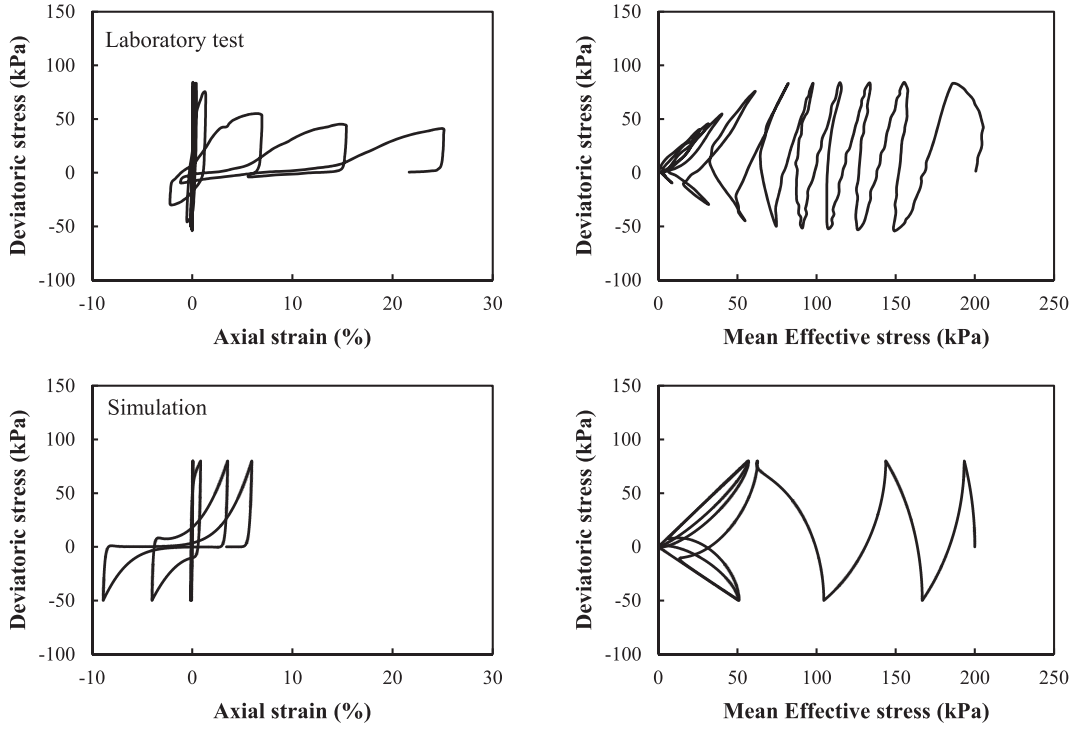

(b) C-30-73, FC = 30%, e_c = 0.454, p_c' = 200 kPa

Fig. 17. Cyclic mobility of Sydney sand series (laboratory data extracted from Rahman et al. (2014), Baki et al. (2012)).

4.1.2. Prediction of non-flow type behavior

Three typical tests exhibiting non-flow type behavior are simulated, corresponding to three different fines contents, namely FC = 0 (Fig. 11), 10% (Fig. 12) and 20% (Fig. 13). All the specimens were isotropically consolidated to achieve nearly the same void ratio ($e_c \approx$ 0.791). Again, a reasonally good agreement is obtained between simulations and experiments. As the mean effective stress approaches zero, the stress paths exhibit butterfly loops. The stress-strain curves also present large deformation when the cyclic deviatoric stress changes its direction. These are typical aspects of the failue pattern known as cyclic mobility.

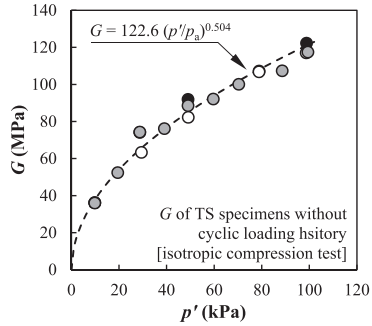

(a) G measured using isotropically consolidated specimens without cyclic loading history

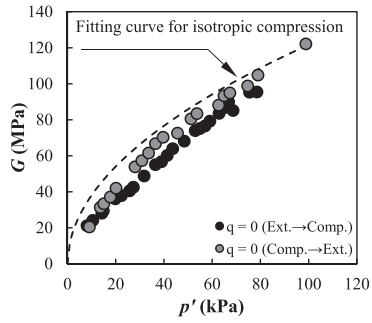

(b) G measured during cyclic loading

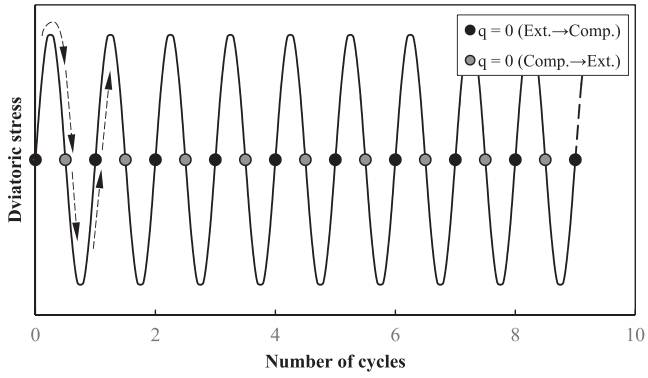

(c) Schematics of the idealized measuring point

Fig. 18. Effects of cyclic loading on small-strain shear modulus (Goto et al., 1999).

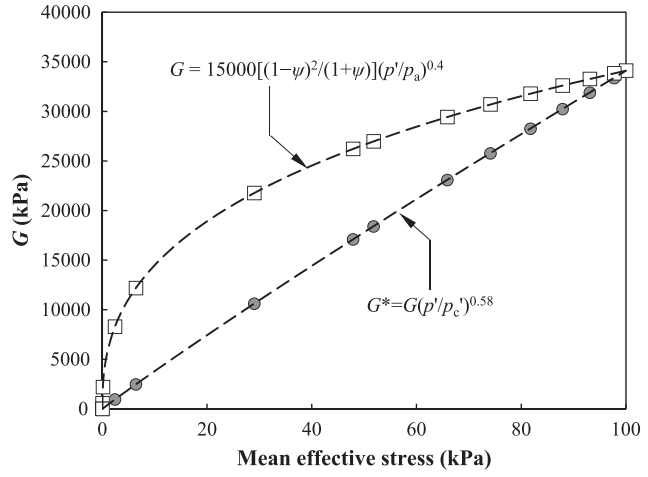

Fig. 19. Small-strain shear modulus in cyclic simulation (G^*) in comparison with the shear modulus under isotropic stress state.

4.1.3. Effects of initial state

It is well known that the mechanical behavior of sands is dependent on the initial state in terms of packing density and effective confining pressure. By comparing the responses in Figs. 8 and 11, in Figs. 9 and 12, and in Figs. 10 and 13, it becomes clear that the failure pattern is highly affected by the void ratio: it turns from flow-type (flow failure) to non-flow type (cyclic mobility) with decreasing void ratio.

The effective confining stress has a certain impact on the liquefaction potential and cyclic behavior of clean and silty sands (Wei and Yang, 2019; Yang and Sze, 2011). For example, two TSS10 specimens with nearly the same void ratio ($e_c \approx 0.791$) were consolidated to 100 kPa (Fig. 14(a)) and 300 kPa (Fig. 14(b)), and then loaded under the same cyclic stress ratio ($q_{cyc}/p_c' = 0.5$, where q_{cyc} is the amplitude of deviatoric stress cycle). To allow a direct comparison of the cyclic behavior under different confining pressures, the mean effective stress and the deviatoric stress are normalized by the post-consolidation mean effective stress (p_c'). Although the failure pattern remains the same (i.e., cyclic mobility) when the effective stress increases from 100 kPa to 300 kPa, the specimen with 300 kPa appears to be more prone to liquefaction in that relatively fewer cycles are required to reach zero effective stress. The simulated results show good agreement with the laboratory test results.

4.1.4. Effects of fines content

In Fig. 15, the simulations of two cases with different fines contents but the same initial state ($e_c = 0.847$, $p_c' = 100$ kPa) are compared with laboratory results. By increasing FC from 10 to 20% (Fig. 15 (a) to (b)), the failure pattern turns from the cyclic mobility (Fig. 15(a)) to flow type behavior (Fig. 15(b)). Note that the only difference between the two cases is the fines content. The observed change of failure pattern is reasonable since cyclic behavior is dependent on the initial state and the addition of fines affects the initial state parameter in the proposed model.

4.2. Sydney sand series

The undrained cyclic triaxial tests reported in Rahman et al. (2014), Baki et al. (2012) are simulated using the proposed model with the calibrated parameters in Table 3. Note that e_Γ decreases and λ_c increases as the fines content increases from 15% to 30%. For simplicity, the critical state stress ratio, M, is assumed to be a constant.

Two samples exhibiting flow-type failure are presented in Fig. 16. Both specimens were subjected to unloading after a certain level of strain softening and then loaded in the compression side as indicated by the dotted lines. The strengths of the samples failed to restore upon shearing, with the effective stress remain zero. If the samples were able to respond to the rapid deformation after the triggering of the flow failure, they would continuously be sheared in the extension side as indicated by the dotted lines in the simulation. Overall, the simulations capture the observed characteristics in a reasonable way.

Two samples exhibiting cyclic mobility are presented in Fig. 17. In both tests, the prescribed amplitudes of stress cycles were not reached in the last few cycles. This is likely due to the slow response of the loading system to the rapid deformation in real tests. Both samples exhibited a strong compressional bias of axial strain development, partly due to the compressional bias of the stress cycles. The additional cause is perhaps the missing extensional stress cycles (negative deviatoric stress) due to the loading system being unable to respond fast to the rapid deformation at the low effective stress state. For both cases, the model predicts the response with uniform stress cycles and hence the strain development is more balanced on both extensional and compressional sides.

5. Discussions

The model presented in this study incorporates the state-parameter-dependent elastic shear modulus and hardening modulus to simulate in

a unified way the cyclic behavior of sands with various fines contents. The simulated responses match reasonably well with the experimental results for a range of fines contents (0–20% for Toyoura series and 15–30% for Sydney sand series) and under a relatively wide range of initial states.

In this model an additional stress exponential term is included into the original expression of the elastic shear modulus G proposed by Yang and Liu (2016). It is added based on the analysis of the laboratory data on variations of G during undrained cyclic triaxial tests (Goto et al., 1999). In these tests, the small-strain shear modulus was first measured using specimens during isotropic compression tests, without any cyclic loading history. The G-p' data exhibit a convex trendline as shown in Fig. 18(a). The small-strain shear modulus was also measured when the deviatoric stress reached zero during the cyclic loading. The G-p' data during the loading are presented in Fig. 18(b), showing a similar but less convex trend. Fig. 18(c) schematically explains how the data points in Fig. 18(b) were measured. The use of the additional stress exponential term helps to capture the characteristics of shear modulus (Fig. 19). In addition, it can also improve the model performance in simulating the large deformation associated with cyclic mobility.

Nevertheless, the fabric of sand, characterized by particle orientation, void characteristics, contact orientation, etc, is not taken into account in the present model. There is a general agreement that the fabric may affect the behavior and liquefaction resistance of granular soils (Zhao and Gao, 2016; Li and Dafalias, 2012; Sze and Yang, 2014; Yang et al., 2008). For example, Sze and Yang (Sze and Yang, 2014) reported that different sample preparation methods lead to different cyclic responses under otherwise similar conditions and that liquefaction resistance of the moist-tamped sample is higher than the counterpart prepared by the dry deposition method. They attributed the different responses to different fabrics formed by the two sample preparation methods. The microscopic investigation of Yang et al. (2008) showed that the moist-tamping method produces less anisotropic fabric than the dry deposition method in terms of particle orientation. In this study, the laboratory data for both calibration and validation were obtained from specimens reconstituted by moist tamping. To account for the fabric effect in future, calibration and validation using specimens reconstituted by other sample preparation methods are needed. In addition, it should be noted that the stress-dilatancy relationship may change during cyclic loading (Pradhan et al., 1989) and this change is related to fabric evolution (Wan and Guo, 2001). How to incorporate a mechanism to properly account for the fabric evolution and its effects on pore pressure generation and the asscciated reduction of effective stress remains a difficult task for future research.

The critical state parameters are FC-specific and generally require a certain amount of laboratory tests for accurate estimates. Several key factors that affect the critical state lines have been identified and some empirical relationhsips have been proposed (Yang and Wei, 2012; Yang and Luo, 2015). Most recently, Yang et al. (2018) proposed an attractive method that allows direct evaluation of initial state parameters of clean and silty sands in a unified way. Another concern is the potential effect of fines content on dilatancy parameters (Xiao et al., 2014). Currently, there is a lack of systematic data for characterizing such effect. The h-ψ_0 correlation presented here is an improved version of the original h-e_0 correlation of Li and Dafalias (2000). This new proposal can enhance the state-parameter-dependence of plastic hardening modulus for silty sands, thus improving the model performance. However, the linear equation is generally empirical and omits the possible curvature of the h-ψ_0 correlation (Wei and Yang, 2019). Further investigation with regard to the above mentioned is worthywhile. A gneralization of the model from the triaxial space to the multi-axial space is also needed.

6. Conclusions

This paper presents a CSSM based constitutive model which allows unified modeling of the cyclic behavior of clean and silty sands. The model incorporates several important findings from recent laboratory experiments, including the state-parameter-dependent elastic modulus and plastic hardening modulus. The model has been shown to be able to simulate a spectrum of undrained cyclic behavior of silty sands with varying fines contents, from flow failure to cyclic mobility, by using the same set of model parameters. A resonablly good agreement between simulations and experiments in terms of stress-strain response and stress path has been confirmed.

The simulations also have shown that the cyclic behavior of silty sands depends on their initial state. With increasing void ratio, the failure pattern can turn from non-flow type (cyclic mobility) to flow type (flow failure). The initial effective confining stress also has a certain impact on the cyclic behavior, but it is relatively less significant compared with that of void ratio for stress levels of practical interest (< 300 kPa). The fines content can affect the position of the critical state line and hence the initial state parameter, and different initial state parameters lead to changes in cyclic behavior. These observations confirm that CSSM is a rational framework for modeling the behavior of clean and silty sands.

CRediT authorship contribution statement

Xiao Wei: Methodology, Formal analysis, Writing - original draft. **Yuan Chen:** Investigation. **Jun Yang:** Conceptualization, Methodology, Supervision, Funding acquisition, Writing - review & editing.

Declaration of Competing Interest

The authors declare that they have no known competing financial interests or personal relationships that could have appeared to influence the work reported in this paper.

Acknowledgment

The financial support provided by the Research Grants Council of Hong Kong (No. 17250316; 17205717) is gratefully acknowledged.

References

Baki, M.A.L., Rahman, M.M., Lo, S.R., Gnanendran, C.T., 2012. Linkage between static and cyclic liquefaction of loose sand with a range of fines contents. Can. Geotech. J. 49, 891–906. https://doi.org/10.1139/t2012-045.

Been, K., Jefferies, M.G., 1985. A state parameter for sands. Géotechnique 35, 99–112.

Borja, R.I., Andrade, J.E., 2006.. Critical state plasticity. Part VI: Meso-scale finite element simulation of strain localization in discrete granular materials. Comput. Methods Appl. Mech. Eng. 195, 5115–5140. https://doi.org/10.1016/j.cma.2005.08.020.

Carraro, J.A.H., Bandini, P., Salgado, R., 2003. Liquefaction resistance of clean and nonplastic silty sands based on cone penetration resistance. J. Geotech. Geoenviron. Eng 129, 965–976. https://doi.org/10.1061/(ASCE)1090-0241(2003)129:11(965).

Dafalias, Y.F., Manzari, M.T., 2004. Simple plasticity sand model accounting for fabric change effects. J. Eng. Mech. 130, 622–634. https://doi.org/10.1061/(ASCE)0733-9399(2004)130:6(622).

Dafalias, Y.F., Taiebat, M., 2016. SANISAND-Z: zero elastic range sand plasticity model. Géotechnique 66, 999–1013. https://doi.org/10.1680/jgeot.15.P.271.

Darve, F., Labanieh, S., 1982. Incremental constitutive law for sands and clays– simulations of monotonic and cyclic tests. Int. J. Numer. Anal. Methods Geomech. 6, 243–275.

Dash, H.K., Sitharam, T.G., 2009. Undrained cyclic pore pressure response of sand–silt mixtures: effect of nonplastic fines and other parameters. Geotech. Geol. Eng. 27, 501–517. https://doi.org/10.1007/s10706-009-9252-5.

Goto, S., Matsueda, S., Morri, Y., Sueoka, T., 1999. Small strain stiffness of sands in isotropic compression and liquefaction tests. 2nd Int Symp Pre-Failure Deform Charact Geomaterials,1:275–81.

Gu, X., Yang, J., Huang, M., 2013. Laboratory measurements of small strain properties of dry sands by bender element. Soils Found 53, 735–745. https://doi.org/10.1016/j.sandf.2013.08.011.

Guo, P., Su, X., 2007. Shear strength, interparticle locking, and dilatancy of granular materials. Can. Geotech. J. 44, 579–591. https://doi.org/10.1139/t07-010.

Huang, Y.-T., Huang, A.-B., Kuo, Y.-C., Tsai, M.-D., 2004. A laboratory study on the undrained strength of a silty sand from Central Western Taiwan. Soil Dyn. Earthq. Eng. 24, 733–743. https://doi.org/10.1016/j.soildyn.2004.06.013.

Iwasaki, T., Tatsuoka, F., 1977. Effects of grain size and grading on dynamic shear moduli of sands. Soils Found 17, 19–35.

Jefferies, M.G., 1993. Nor-Sand: a simple critical state model for sand. Géotechnique 43, 91–103. https://doi.org/10.1680/geot.1993.43.1.91.
Kuerbis, R.H., Negussey, D., Vaid, Y.P., 1988. Effect of gradation and fines content on the undrained response of sand. A Spec Conf Hydraul Fill Struct, pp. 330–345.
Li, X.S., 2002. A sand model with state-dependent dilatancy. Géotechnique 52, 173–186. https://doi.org/10.1680/geot.2002.52.3.173.
Li, X.S., Dafalias, Y.F., 2000. Dilatancy for cohesionless soils. Géotechnique 50, 449–460. https://doi.org/10.1680/geot.2000.50.4.449.
Li, X.S., Dafalias, Y.F., 2012. Anisotropic critical state theory: role of fabric. J. Eng. Mech. 138, 263–275. https://doi.org/10.1061/(ASCE)EM.1943-7889.0000324.
Li, X.S., Wang, Y., 1998. Linear representation of steady-state line for sand. J. Geotech. Geoenviron. Eng. 124, 1215–1217. https://doi.org/10.1061/(ASCE)1090-0241(1998)124:12(1215).
Liang, L., 2016. Static Liquefaction of Sand-Fines Mixtures with the Presence of Initial Shear Stress. MPhil Thesis. The University of Hong Kong.
Ling, H.I., Liu, H., 2003. Pressure-level dependency and densification behavior of sand through generalized plasticity model. J. Eng. Mech. 129, 851–860. https://doi.org/10.1061/(ASCE)0733-9399(2003)129:8(851).
Ling, H.I., Yang, S., 2006. Unified sand model based on the critical state and generalized plasticity. J. Eng. Mech. 132, 1380–1391. https://doi.org/10.1061/(ASCE)0733-9399(2006)132:12(1380).
Manzari, M.T., Dafalias, Y.F., 1997. A critical state two-surface plasticity model for sands. Géotechnique 47, 255–272. https://doi.org/10.1680/geot.1997.47.2.255.
Papadimitriou, A.G., Bouckovalas, G.D., Dafalias, Y.F., 2001. Plasticity model for sand under small and large cyclic strains. J. Geotech. Geoenviron. Eng. 127, 973–983. https://doi.org/10.1061/(ASCE)1090-0241(2001)127:11(973).
Pastor, M., Zienkiewicz, O.C., Chan, A.H.C., 1990. Generalized plasticity and the modelling of soil behaviour. Int. J. Numer. Anal. Methods Geomech. 14, 151–190. https://doi.org/10.1002/nag.1610140302.
Potts, D.M., Zdravković, L., 2001. Finite Element Analysis in Geotechnical Engineering: Theory. vol. 1. Thomas Telford; 2001.
Pradhan, T.B.S., Tatsuoka, F., Sato, Y., 1989. Experimental stress-dilatancy relations of sand subjected to cyclic loading. Soils Found 29, 45–64. https://doi.org/10.3208/sandf1972.29.45.
Rahman, M.M., Baki, M.A.L., Lo, S.R., 2014. Prediction of undrained monotonic and cyclic liquefaction behavior of sand with fines based on the equivalent granular state parameter. Int. J. Geomech. 14, 254–266. https://doi.org/10.1061/(ASCE)GM.1943-5622.0000316.
Shen, C.K., Vrymoed, J.L., Uyeno, C.K., 1977. The effects of fines on liquefaction of sands. In: 9th Int Conf Soil Mech Found Eng, pp. 381–386.
Simoni, A., Houlsby, G.T., 2006. The direct shear strength and dilatancy of sand–gravel mixtures. Geotech. Geol. Eng. 24, 523–549. https://doi.org/10.1007/s10706-004-5832-6.
Stamatopoulos, C.A., 2010. An experimental study of the liquefaction strength of silty sands in terms of the state parameter. Soil Dyn. Earthq. Eng. 30, 662–678. https://doi.org/10.1016/j.soildyn.2010.02.008.
Stamatopoulos, C.A., Lopez-Caballero, F., Modaressi-Farahmand-Razavi, A., 2015. The effect of preloading on the liquefaction cyclic strength of mixtures of sand and silt. Soil Dyn. Earthq. Eng. 78, 189–200. https://doi.org/10.1016/j.soildyn.2015.07.004.
Sze, H.Y., Yang, J., 2014. Failure modes of sand in undrained cyclic loading: impact of sample preparation. J. Geotech. Geoenviron. Eng. 140, 152–169. https://doi.org/10.1061/(ASCE)GT.1943-5606.0000971.
Taiebat, M., Dafalias, Y.F., 2008. SANISAND: simple anisotropic sand plasticity model. Int. J. Numer. Anal. Methods Geomech. 32, 915–948.
Thevanayagam, S., Fiorillo, M., Liang, J., 2000. Effect of non-plastic fines on undrained cyclic strength of silty sands. Soil Dyn. Liq. 77–91.
Wan, R.G., Guo, P.J., 2001. Drained cyclic behavior of sand with fabric dependence. J. Eng. Mech. 127, 1106–1116. https://doi.org/10.1061/(ASCE)0733-9399(2001)127:11(1106).
Wang, Z.L., Dafalias, Y.F., Shen, C.K., 1990. Bounding surface hypoplasticity model for sand. J. Eng. Mech. 116, 983–1001.
Wang, G., Xie, Y., 2014. Modified bounding surface hypoplasticity model for sands under cyclic loading. J. Eng. Mech. 140, 91–101. https://doi.org/10.1061/(ASCE)EM.1943-7889.0000654.
Wei, X., Yang, J., 2019. Cyclic behavior and liquefaction resistance of silty sands with presence of initial static shear stress. Soil Dyn. Earthq. Eng. 122, 274–289. https://doi.org/10.1016/j.soildyn.2018.11.029.
Wei, X., Yang, J., 2019. A critical state constitutive model for clean and silty sand. Acta Geotech. 14, 329–345. https://doi.org/10.1007/s11440-018-0675-0.
Wichtmann, T., Navarrete Hernández, M.A., Triantafyllidis, T., 2015. On the influence of a non-cohesive fines content on small strain stiffness, modulus degradation and damping of quartz sand. Soil Dyn. Earthq. Eng. 69, 103–114. https://doi.org/10.1016/j.soildyn.2014.10.017.
Wichtmann, T., Triantafyllidis, T., 2009. Influence of the grain-size distribution curve of quartz sand on the small strain shear modulus Gmax. J. Geotech. Geoenviron. Eng. 135, 1404–1418. https://doi.org/10.1061/(ASCE)GT.1943-5606.0000096.
Wood, D.M., 1990. Soil Behaviour and Critical State Soil Mechanics. Cambridge University Press.
Xenaki, V.C., Athanasopoulos, G.A., 2003. Liquefaction resistance of sand–silt mixtures: an experimental investigation of the effect of fines. Soil Dyn. Earthq. Eng. 23, 1–12. https://doi.org/10.1016/S0267-7261(02)00210-5.
Xiao, Y., Liu, H., Chen, Y., Chu, J., 2014. Strength and dilatancy of silty sand. J. Geotech. Geoenviron. Eng. 140, 6014007. https://doi.org/10.1061/(ASCE)GT.1943-5606.0001136.
Yang, J., 2002. Non-uniqueness of flow liquefaction line for loose sand. Géotechnique 52, 757–760.
Yang, J., Li, X., 2004. State-dependent strength of sands from the perspective of unified modeling. J. Geotech. Geoenviron. Eng. 130, 186–198. https://doi.org/10.1061/(ASCE)1090-0241(2004)130:2(186).
Yang, Z.X., Li, X.S., Yang, J., 2008. Quantifying and modelling fabric anisotropy of granular soils. Géotechnique 58, 237–248.
Yang, J., Liu, X., 2016. Shear wave velocity and stiffness of sand: the role of non-plastic fines. Géotechnique 66, 500–514. https://doi.org/10.1680/jgeot.15.P.205.
Yang, J., Wei, L.M., Dai, B.B., 2015. State variables for silty sands: global void ratio or skeleton void ratio? Soils Found 55, 99–111. https://doi.org/10.1016/j.sandf.2014.12.008.
Yang, J., Liu, X., Guo, Y., Liang, L.B., 2018. A unified framework for evaluating in situ state of sand with varying fines content. Géotechnique 68, 177–183.
Yang, J., Luo, X.D., 2015. Exploring the relationship between critical state and particle shape for granular materials. J. Mech. Phys. Solids 84, 196–213. https://doi.org/10.1016/j.jmps.2015.08.001.
Yang, J., Sze, H.Y., 2011. Cyclic behaviour and resistance of saturated sand under non-symmetrical loading conditions. Géotechnique 61, 59–73. https://doi.org/10.1680/geot.9.P.019.
Yang, J., Wei, L.M., 2012. Collapse of loose sand with the addition of fines: the role of particle shape. Géotechnique 62, 1111–1125. https://doi.org/10.1680/geot.11.P.062.
Yang, Z.X., Xu, T.T., Li, X.S., 2019. J2-deformation type model coupled with state dependent dilatancy. Comput. Geotech. 105, 129–141. https://doi.org/10.1016/j.compgeo.2018.09.018.
Zhang, J.-M., Wang, G., 2012. Large post-liquefaction deformation of sand, part I: physical mechanism, constitutive description and numerical algorithm. Acta Geotech. 7, 69–113. https://doi.org/10.1007/s11440-011-0150-7.
Zhao, J., Gao, Z., 2016. Unified anisotropic elastoplastic model for sand. J. Eng. Mech. 142. https://doi.org/10.1061/(ASCE)EM.1943-7889.0000962.